Mammalian glial protrusion transcriptomes predict localization of *Drosophila* glial transcripts required for synaptic plasticity

DALIA S. GALA[1*], JEFFREY Y. LEE[1*], MARIA KIOURLAPPOU[1], JOSHUA S. TITLOW[1], RITA O. TEODORO[2], ILAN DAVIS[1]

Authors institutional affiliations

1 Department of Biochemistry, The University of Oxford, UK

2 NOVA Medical School - Faculdade de Ciências Médicas, Universidade Nova de Lisboa, Portugal

* these authors contributed equally to the work

SUMMARY (150 words)

The polarization of cells often involves the transport of specific mRNAs and their localized translation in distal projections. Neurons and glia both contain long cytoplasmic processes with important functions. mRNA localization has been studied extensively in neurons, but very little in glia, especially in intact nervous systems. Here, we predicted 1,700 localized *Drosophila* glial transcripts by extrapolating from our meta-analysis of 8 existing studies characterizing the localized transcriptomes and translatomes of synaptically-associated mammalian glia. We tested these predictions in glia of the neuromuscular junction of *Drosophila* larvae and found that localization to mammalian glia is a strong predictor of mRNA localization of the high confidence *Drosophila* homologues. We further showed that some of these localized transcripts are required in glia for plasticity of the neuromuscular junction synapses. We conclude that peripheral glial mRNA localization is a common and conserved phenomenon and propose that it is likely to be functionally important.

KEYWORDS:

Drosophila, glia, mRNA transport, mRNA, mRNA localization, localized translation

1 INTRODUCTION

It is well established that specific mRNAs are actively transported and localized to distal compartments of neurons, including those encoding cytoskeletal proteins, neurotransmitters, membrane proteins and ribosomes. In these studies, mRNA transport and local translation have been proposed as mechanisms for local regulation of synaptic plasticity, which is the process underlying memory and learning (Smith, Aakalu and Schuman, 2001; Sutton and Schuman, 2006; Wang, Martin and Zukin, 2010; Daniel E Shumer, 2017; Rangaraju, tom Dieck and Schuman, 2017; Terenzio, Schiavo and Fainzilber, 2017; Biever, Donlin-Asp and Schuman, 2019; Holt, Martin and Schuman, 2019; Wang *et al.*, 2009).

Asymmetric mRNA localization is likely to be as important in glia, as it is in neurons, but has received very little attention in glia. Like neurons, glial cells can display diverse morphologies ranging from immune-cell-like microglia, to elongated myelinating oligodendrocytes and astrocytes that contact thousands of synapses. Therefore, astrocytes are thought to integrate information from distinct neuronal populations (Ransom and Ransom, 2012; Jessen, Mirsky and Lloyd, 2015; Allen and Lyons, 2018; Volterra and Meldolesi, 2005). Astrocytes also perform key roles in the uptake and release of neurotransmitters and the maintenance of ionic balance. Glia form the blood-brain barrier that regulates neuronal metabolism and local solute homeostasis, as well as secretion of gliotransmitters and mediation of signaling pathways (De Pittà, Brunel and Volterra, 2016; Wang, Fu and Ip, 2022; Ota, Zanetti and Hallock, 2013). Oligodendrocytes are thought to modulate synaptic plasticity via myelination (Fields, 2005; Fields, 2008; de Faria *et al.*, 2021; Bacmeister *et al.*, 2020; Pan *et al.*, 2020; Fields and Bukalo, 2020). Microglia can preferentially phagocytose synaptic endings and modulate connectivity in the visual cortex (Andoh and Koyama, 2021; Graeber, 2010; Morris *et al.*, 2013; Schafer *et al.*, 2012; Vasek *et al.*, 2021). All of these functions occur in remote cellular processes that are separated from the core gene expression machinery in the cell body. Although these varying glial morphologies and functional roles are suggestive of mRNA localization (Blanco-Urrejola *et al.*, 2021; Meservey, Topkar and Fu, 2021), it is not clear whether mRNA localization is common in glia, nor whether a common set of mRNAs exists that localizes to the periphery of most of the glial sub-types or in neurons. It is also

not known whether such glial mRNA localization is conserved and functionally important.

To address these questions, we have carried out a meta-analysis of, to our knowledge, all the published mammalian glial peripheral or synaptic transcriptomes and translatomes. We found several classes of mRNAs that are localized in multiple glial subtypes and determined a common set of 4801 transcripts present in the majority of the analyzed libraries, representing multiple types of mammalian glial cells. We used this cohort to find high confidence *Drosophila* homologues and filtered the list for glial expression using the Fly Cell Atlas data, a single-cell nuclear sequencing atlas derived from entire adult flies (Li *et al.*, 2022). We specifically selected for expression in 3 glial subtypes known to create distal protrusions in the larval NMJ, namely perineural, subperineural and wrapping glia, which are continuous with the ensheathing glia in the PNS (Yildirim *et al.*, 2019; Sepp, Schulte and Auld, 2000), resulting in 1,700 mRNAs predicted to be localized in these three glial subtypes.

To test our predictions of mRNA localization in *Drosophila* glial projections, we studied in greater detail 15 conserved transcripts, which in an unrelated survey of 200 transcripts across the nervous system, we discovered were likely to be localized at glial distal projections near the NMJ axonal synapses (Titlow *et al.*, 2022). We first confirmed that these 15 transcripts were indeed localized, using definitive glial markers and more extensive, higher precision 3D microscopy. We then determined whether these experimentally determined localized transcripts are predicted as localized from our meta-analysis. We found that more than 70% (11 of the 15) conserved localized transcripts were correctly predicted as localized, through being in the list of 1,700 transcripts. Furthermore, in follow up experiments, we tested whether the localized transcripts are required in the glia for the correct plasticity of the adjacent neuronal synapses, using a spaced potassium stimulation assay (Ataman *et al.*, 2008; Roche *et al.*, 2002). We found that 5 of the 15 localized transcripts impaired synaptic plasticity in the neighboring wild type neurons, reducing their ability to make new synapses. Our results suggest that mRNA localization to protrusions represent an important and conserved mechanism that allows glia to rapidly regulate the plasticity of adjacent distal axonal synapses.

2 MATERIALS AND METHODS

2.1 Data meta-analysis methods

We developed a custom RNA-seq analysis pipeline to process public transcriptomic datasets and allow the integration of diverse raw datasets from 8 different studies. Raw FASTQ files were downloaded from Gene Expression Omnibus (GEO) and were filtered to remove ribosomal RNA reads using BBduk (Bushnell, Rood and Singer, 2017). Processed reads were mapped to *Mus musculus* (ENSEMBL release 96) or *Rattus norvegicus* (ENSEMBL release 98) genomes using Kallisto to obtain Transcripts per million (TPM) abundance measures (Bray *et al.*, 2016). A TPM value > 10 for a transcript was considered a transcript to be present in a given compartment. In order to take into account intronic reads in libraries derived from soma, Kallisto bustools was used to create transcriptome indices containing intron sequences (Melsted *et al.*, 2021). For the relative enrichment analysis comparing soma and protrusion compartments, DESeq2 was used to assess differential expression of transcripts from estimated transcript counts output (Love, Huber and Anders, 2014). The independent hypothesis weighting (IHW) method was used to correct for the multiple testing (Ignatiadis *et al.*, 2016), and the adjusted p-value<0.01 & log2FoldChange>0 was considered significantly enriched.

For the datasets where raw data were unavailable, the reported HTSeq count table was used as input for DESeq2, and the conflicting transcript annotations between ENSEMBL releases were manually resolved. In the case of non-Illumina-based sequencing datasets, numerical log2foldchange was calculated from the reported TPMs of each gene. *R. norvegicus* datasets were converted to *M. musculus* genes using ENSEMBL BioMart annotations after the differential expression processing. All summary data obtained from our analysis is available in Supplementary Table 1.

Gene Ontology (GO) enrichment analyses were performed using a Bioconductor package TopGO (Alexa and Rahnenfuhrer, 2022). To prevent artefactual enrichment of brain-related terms, adult mouse brain transcriptome (Accession number: ENCFF468CXD) from the ENCODE project was used as background. Multiple testing was corrected via the Bonferroni method. An adjusted p-value<0.05 and foldchange>2 was considered a significant enrichment. Summaries of enriched GO terms were processed using the R package SimplifyEnrichment (Gu and

Hübschmann, 2022) via clustering significantly enriched GO terms based on semantic similarity. Unclustered individual GO terms are given in Figure S2 and Supplementary Table 2

Conversion between human, mouse and fly orthologues (ENSEMBL release 99) was performed using the source data of DIOPT version 9 (Hu *et al.*, 2011). To select for high-confidence orthologues, a cut-off score of 8 was used. Fly genes with the associated disease ontologies were acquired from FlyBase, and the enrichment of disease ontology terms were assessed with hypergeometric test followed by Bonferroni's method multiple hypothesis correction.

To identify transcripts that are expressed in the three glial cell types (perineurial, subperineurial and ensheathing glial cells), single-cell nucleus sequencing data from Fly Cell Atlas was used (Li *et al.*, 2022). The 'Glial Cell' loom file from 10x Cross-Tissue dataset was downloaded and filtered for non-glial cells based on the annotation. Using the R package ScopeLoomR (https://github.com/aertslab/SCopeLoomR), the digital gene expression matrices for the three cell types were extracted and the transcripts expressed in at least 5% of the corresponding clusters were identified.

For the Reactome pathway enrichment analysis, the gene to pathway query from Flymine was used to extract the Reactome ID annotations for each gene (https://www.flymine.org/flymine/templates/Gene_Pathway). The Reactome pathway hierarchical relationship between terms (available here) was used to group genes to the two highest hierarchical levels, the "top-level pathways" and the next hierarchical level, the "sub-pathways", was used to calculate the enrichment.

All analysis scripts and data produced from this study are available at https://github.com/jefflee1103/Gala2023_glia-localised-RNA. The data that supports the findings of this study are available in the supplementary material of this article.

2.2 Experimental methods

2.2.1 Fly stocks

The fly lines used in this research were raised at 25ºC (all stocks used in the smFISH experiments and the spaced potassium assay experiment apart from *Nrg*-

RNAi) or 30ºC (larvae used for the *Nrg*-RNAi spaced potassium assay experiment in glial cells) on a standard cornmeal-agar food. To label glial cells in the smFISH experiments, a cross was made to obtain the following stock: UAS-mCD8-mCherry/CyoGFP; Repo>GAL4/Tm6B, Tb. This stock was then crossed to each of the CPTI lines and offspring selected for YFP and mCherry fluorescence. To label glia in the spaced potassium assay experiment with RNAi of transcripts of interest in glial cells, the following stock was constructed: UAS-mCD8-GFP/UAS-mCD8-GFP; Repo>GAL4/Tm6B, Tb. For each RNAi experiment, a homozygous line where a hairpin targets the coding sequence of the gene of interest with least number of off-targets was selected. If the progeny of the RNAi cross was embryonic or larval lethal, the next most suitable RNAi line meeting the above criteria was used. These lines were then crossed to the UAS-mCD8-GFP/UAS-mCD8-GFP; Repo-GAL4/Tm6B, Tb, and offspring selected for GFP fluorescence and lack of Tm6B, Tb phenotype. The control for the UAS-RNAi experiment was UAS-mCD8-GFP/+; Repo-GAL4/UAS-mCherry-RNAi. The glial cell specific knockdown of the 11 localized transcripts resulted in lethality for *Cip4*, where no 3rd instar Drosophila larvae of the correct genotype were observed. For Atpalpha (GD3093) and *Lac* (KK107450), the UAS-RNAi larvae were extremely few, small and sickly, and the experiments could not be performed on them. Using other UAS-RNAi lines for *Atpalpha* (HMS00703) and *Lac* (GD35524) allowed us to continue with experiments on those knockdown larvae. We observed no adults of the UAS-RNAi genotype for *nrv2*-RNAi, *Lac*-RNAi, *Cip4*-RNAi, and *Vha55*-RNAi. We observed adults for all other Repo>UAS-RNAi. crosses. **Table 1** lists all the strains used in the study.

Line name	Line ID	Line source	Line description
nrv2::YFP	CPTI001455	Kyoto Stock Centre - Drosophila Genomics and Genetic Resources (DGRC) (https://www.dgrc.kit.ac.jp/)	*Nervana 2* gene YFP protein trap line ((Lowe *et al.*, 2014)
Flo-2::YFP	CPTI001427	DGRC	*Flotillin 2* gene YFP protein trap line
Cip4::YFP	CPTI003231	DGRC	*Cdc42-interacting protein 4* gene YFP protein trap line
Vha55::YFP	CPTI002645	DGRC	*Vacuolar H+-ATPase 55kD subunit* gene YFP protein trap line
Atpalpha::YFP	CPTI002636	DGRC	*Na pump α subunit* gene YFP protein trap line
Nrg::YFP	CPTI002761	DGRC	*Neuroglian* gene YFP protein trap line
Lac::YFP	CPTI001714	DGRC	*Lachesin* gene YFP protein trap line
alpha-Cat::YFP	CPTI002408	DGRC	*α Catenin* gene YFP protein trap line

Pdi::YFP	CPTI002342	DGRC	*Protein disulfide isomerase* gene YFP protein trap line
gs2::YFP	CPTI001918	DGRC	*Glutamine synthetase 2* gene YFP protein trap line
Repo-GAL4	RRID:BDSC_7415	Bloomington Drosophila Stock Center (BDSC) (https://bdsc.indiana.edu/index.html)	Expresses GAL4 in glia
UAS-mCD8-mCherry/cyo-GFP	RRID:BDSC_27391	BDSC	Expresses Cherry RFP fused to the mouse CD8 extracellular and transmembrane domains for membrane targeting under UAS control.
UAS-mCD8-GFP/cyo-GFP	RRID:BDSC 63045	BDSC	Expresses GFP fused to the mouse CD8 extracellular and transmembrane domains for membrane targeting under UAS control.
cyo-GFP/Gla; tm6, tb/pri	Crossed from BDSC stocks	BDSC	A double balanced stock carrying Cyo-GFP over Gla on the 2nd chromosome and tm6, tb over prickle on the 3rd chromosome.
Atpalpha-RNAi	RRID:BDSC 32913	BDSC	Expresses dsRNA for RNAi of Atpalpha under UAS control in the VALIUM20 vector.
Atpalpha-RNAi	GD3093	Vienna Drosophila Resource Center (VDRC)	Expresses dsRNA for RNAi of Atpalpha under UAS control in the pUAST vector pMF3.
alpha-Cat-RNAi	KK107298	VDRC	Expresses dsRNA for RNAi of *alpha-Cat* under UAS control in the pUAST vector pMF3.
nrv2-RNAi	GD960	VDRC	Expresses dsRNA for RNAi of *nrv2* under UAS control in the pUAST vector pMF3.
shot-RNAi	RRID:BDSC 28336	BDSC	Expresses dsRNA for RNAi of shot under UAS control in the VALIUM10 vector.
Vha55-RNAi	GD 9363	VDRC	Expresses dsRNA for RNAi of *Vha55* under UAS control in the pUAST vector pMF3.
Lac-RNAi	GD 35524	VDRC	Expresses dsRNA for RNAi of *Lac* under UAS control in the pUAST vector pMF3.
Lac-RNAi	KK 107450	VDRC	Expresses dsRNA for RNAi of *Lac* under UAS control in the pUAST vector pMF3.
Flo-2-RNAi	VSH 330316	VDRC	Expresses dsRNA for RNAi of *Flo-2* under UAS control in the WALIUM20 vector.
gs2-RNAi	GD 9378	VDRC	Expresses dsRNA for RNAi of *gs2* under UAS control in the pUAST vector pMF3.
Pdi-RNAi	GD13418	VDRC	Expresses dsRNA for RNAi of *Pdi* under UAS control in the pUAST vector pMF3.
mCherry-RNAi	RRID:BDSC 35785	BDSC	Expresses dsRNA for RNAi of mCherry under UAS control in the VALIUM20 vector.
nrv2-GAL4	RRID: BDSC 6800	BDSC	Expresses GAL4 in wrapping glia.
46F-GALl4	-	Gift from Dr. Stefanie Schirmeier	Expresses GAL4 in perineurial glia (Xie and Auld, 2011).
Mdr65-GAL4	RRID: BDSC 50472	BDSC	Expresses GAL4 in subperineurial glia.

Table 1. List of *Drosophila melanogaster* lines which were utilized in this project.

2.2.2 Solutions and reagents

The Haemolymph-Like Salines (HL3 solutions) were prepared as described previously (Roche *et al.*, 2002; Ataman *et al.*, 2008). The list of all the solutions used is given below (**Table 2**).

Solution	**Composition**
HL3 0.3 mM Ca^{2+}+	NaCl 70 mM, KCl 5 mM, $MgCl_2$ 20 mM, $NaHCO_3$ 10 mM, trehalose 5 mM, HEPES 5 mM, sucrose 115 mM, Ca^{2+} 0.3 mM, pH 7.2

HL3 1 mM Ca^{2+}	NaCl 70 mM, KCl 5 mM, $MgCl_2$ 20 mM, $NaHCO_3$ 10 mM, trehalose 5 mM, HEPES 5 mM, sucrose 115 mM, Ca^{2+} 1 mM, pH 7.2
HL3 high K^+	NaCl 40 mM, KCl 90 mM, Ca^{2+} 1.5 mM, $MgCl_2$ 20 mM, $NaHCO_3$ 10 mM, trehalose 5 mM, HEPES 5 mM, sucrose 5 mM, pH 7.2
10x PBS	1.37 M NaCl, 27mM KCl, 100mM Na_2HPO_4, 20mM KH_2PO_4, pH 7.4
PBSTx	PBS 1x, 0.3% Triton X (v/v)
20xSSC	20g NaCl, 100.5g Tri-Sodium Citrate, pH 7.0 in 1L
TE	10 mM Tris-HCL, 1mM EDTA, pH 8.0

Table 2. A list of all the solutions used in the project.

2.2.3 smFISH probes

Probes for the smFISH protocol were designed using a protocol described before (Gaspar, Wippich and Ephrussi, 2017). A set of oligonucleotides (28 for the YFP exon) against the gene region of interest was composed using LGC Biosearch Technologies' Stellaris® RNA FISH Probe Designer. The oligonucleotides were pooled and elongated overnight at 37ºC with a ddUTP conjugated to a desired dye (Atto 633 for the YFP probe) using terminal deoxynucleotidyl transferase enzyme from Life Technologies (Thermo Fisher Scientific). The fluorescently labelled oligonucleotides were then purified by Oligo Clean & Concentrator kit (Zymo Research®) and eluted in TE buffer, after which their concentration and degree of labelling were measured using a NanoDrop spectrophotometer. The probes were diluted with TE buffer to 25µM concentration.

2.2.4 RNA single molecule *in situ* hybridization (smFISH) on the *Drosophila* larval fillet

RNA single molecule in situ hybridization (smFISH) was carried out as described previously (Titlow *et al.*, 2018). In short, wandering 3rd instar (L3) larvae were dissected in HL3 0.3 mM Ca^{2+} as described before to produce a larval fillet with exposed NMJs (Brent, Werner and McCabe, 2009), fixed for 30 minutes at room temperature (RT) using 4% paraformaldehyde in PBS containing 0/1% Triton-X (PBSTx) and permeabilized 2x for 20 minutes in PBSTx at RT. Samples were then pre-hybridized for 20 minutes at 37ºC in wash buffer (2x SSC, 10% formamide (Sigma-Aldrich, F9037)), and then hybridized overnight at 37ºC in hybridization

buffer (10% formamide, 10% dextran sulphate (J62787.18, Alfa Aesar), 250nM smFISH probe(s), anti-HRP (**Table 3**) in 2x SSC). Samples were then rinsed in wash buffer again and counterstained with DAPI (1:1000 from 0.5mg/mL stock) in wash buffer for 45 minutes at RT. Next, samples were washed for 45 minutes in wash buffer at RT and incubated in Vectashield anti-fade mounting medium (Vector Laboratories) adjusted for the objective refractive index for 30 minutes, and subsequently mounted on the slide in the mounting medium.

2.2.5 Immunofluorescence (IF) on the *Drosophila* larval fillet

L3 larvae were dissected and fixed as described in the smFISH protocol. Larvae were then blocked for more than 1 hour at 4ºC in blocking buffer (PBSTx, 1.0% BSA). Samples were incubated overnight at 4ºC with the primary antibody (**Table 3**) in blocking buffer. The next day, samples were washed for about 1 hour and incubated in the secondary antibody solution (conjugated to Alexa Fluor 488, 568 or 647, used at 1:500, from Life Technologies, diluted in PBSTx) together with DAPI (1:1000 from 0.5mg/mL stock) for a further 1 hour. Samples were then washed for 45 minutes in PBSTx at RT and incubated in Vectashield and mounted as in the smFISH protocol (section 2.2.4).

Antibody	Detects	Source	Species	Dilution
Anti-Dlg1	Disks large, a post-synaptic scaffolding protein	Developmental Studies Hybridoma Bank, https://dshb.biology.uiowa.edu/	Mouse	1:200
Anti-HRP conjugated to Alexa 405, 488, 568 or 647	Neurons	Jackson ImmunoResearch Europe Ltd	Goat	1:100

Table 3. A list of all the primary antibodies used in this study.

2.2.6 Spaced High K^+ depolarization paradigm

The spaced potassium assay has been carried out as described before (Piccioli and Littleton, 2014; Roche *et al.*, 2002; Ataman *et al.*, 2008). Briefly, the larvae were dissected in 0.3 mM Ca^{2+} HL3 and then moved to 1 mM Ca^{2+} HL3. The unstretched larvae were then washed with high K^+ HL3 for the periods of 2, 2, 2, 4 and 6 minutes with 15 minutes intervals of 1 mM Ca^{2+} HL3 in between (for RNAi knockdown experiments on *Atpalpha*, *alpha-Cat*, *nrv2*, *shot*, *Nrg*, *Flo-2*, *Vha55*), or periods of 2 minutes, three times, with 10 minutes in between (for RNAi knockdown experiments

on *Lac*, *gs2*, *Pdi*). The assay was performed with a minimum of 5 control and 5 RNAi larvae per each experiment and in one replicate for knockdown of *Atpalpha*, *alpha-Cat*, *Vha55*, two replicates for knockdown of *Nrg* and *Flo-2*, six replicates for the knockdown of *Lac*, three replicates for all remaining RNAi knockdown experiments. In each experiment, an internal control was performed at the same time, where the Repo>mCD8-GFP larvae were crossed to UAS-RNAi line against mCherry protein, absent in these larvae, and each experiment was compared to its internal control only. After the spaced potassium pulses, the larvae were then stretched again, left for a period of rest of 30 minutes, and fixed and labelled as described in the IF protocol. For all experiments, segments A2-A5 of muscles 6/7 were imaged.

2.2.7 Image acquisition and processing

For smFISH experiments, the larvae were dissected, fixed and stained with DAPI and anti-HRP antibody conjugated to the DyLight 405 dye, and the anti-YFP exon probe conjugated to Atto-633 dye, as per the smFISH protocol. A minimum of 3 larvae and 15 NMJs were assessed. For the potassium stimulation experiments, a minimum of 5 control and 5 RNAi larvae were dissected, treated as described above (see “Spaced High K^+ depolarization paradigm”) fixed and stained with DAPI and anti-HRP antibody conjugated to Alexa-647 dye, and the anti-Dlg1 antibody as described in the IF protocol, and the glial membrane was labelled in endogenously with Repo>mCD8-GFP. Mounted specimens were imaged using an inverted Olympus FV3000 laser scanning confocal microscope or Olympus CSU-W1 SoRa laser spinning disk confocal microscope. Images were acquired using 60x 1.4NA Oil UPlanSApo objective (FV3000) or 100x 1.51NA Oil UPlanSApo objective, 100x 1.4NA Oil UPlanSApo objective or 60x 1.51NA Oil UPlanSApo objective (SoRa). Laser units were solid state 405, 488, 568 and 640 lasers for both microscopes.

The images were then processed in ImageJ (https://imagej.nih.gov/ij/) (Schneider, Rasband and Eliceiri, 2012). The glial processes at the NMJ are largely flat, hence the 2 dimensional areas of the GFP labelled glial membranes were measured as previously described; these membranes included small sections of non-synaptic motor axon branches from full Z-stack 2D projections as well as glial membrane nearing the synaptic lamella (Brink *et al.*, 2012b). The neurite areas were measured

identically, except they were labelled with anti-HRP. The settings used were: the linear auto-contrast, auto-threshold, and area measurement functions of NIH ImageJ (Abràmoff, Magalhães and Ram, 2004). In the spaced potassium stimulation experiment, the ghost boutons were quantified manually.

For statistical analysis, R Studio was used. Each two-dimensional area from each NMJ at muscles constituted an independent replicate ("n") value. The n numbers for each genotype and experiment are specified in respective figure legends. For spaced potassium stimulation experiment, we quantified and reported average log2 foldchange of bouton counts post potassium stimulation compared to RNAi controls and performed the Wilcoxon rank sum test. For the areas' quantification, we calculated foldchange in glial protrusion area, neurite area and their ratio upon knock-down of glial protrusion-localized transcripts. We performed these calculations in two sets: before and after potassium activation assay. For each set, average foldchange for each gene was calculated. Student's t-tests were performed on the data to assess significant differences. The summary statistics are available in Supplementary Table 1 (unstimulated NMJs areas), Supplementary Table 1 (stimulated NMJs areas) and Supplementary Table 3 (stimulated NMJs ghost boutons).

3 RESULTS

3.1 Collation of multiple studies characterizing transcript localization to peripheral glial cytoplasmic projections

To identify a common set of localized glial transcripts, we performed a meta-analysis of, to our knowledge, all published mammalian localized and synaptic transcriptomic datasets derived from multiple types of glia (Thomsen *et al.*, 2013; Thakurela *et al.*, 2016; Boulay *et al.*, 2017; Sakers *et al.*, 2017; Azevedo *et al.*, 2018; Mazaré *et al.*, 2020; Vasek *et al.*, 2021), outlined in **Table 4.** Our first goal was to integrate all the raw data, make it interoperable and collate it into a unified data set that can be interrogated as a single entity.

Reference	Cell type	Specimen type	Type of data	Organism
Azevedo *et al.*, 2018	Oligodendrocytes protrusions (OPCs)	Primary cultures of OPCs from rat brain in Boyden Chamber	Soma and protrusion transcriptome	Rat
Thomsen *et al.*, 2013	Perisynaptic astrocytic processes (PAPs)	Type 2 astrocyte mouse cell line C8-S in Boyden Chamber	Soma and protrusion transcriptome	Mouse
Thakurela *et al.*, 2016	Mouse CNS myelin (oligodendrocytes)	Biochemically purified myelin from whole brains of male c57Bl6/N mice	Myelin transcriptome at various developmental stages (P18, P75, 6 and 24 months)	Mouse
Boulay *et al.*, 2017	Astrocyte endfeet	Mechanically isolated brain vessels with attached astrocytic endfeet	Soma and protrusion translatome	Mouse
Sakers *et al.*, 2017	Perisynaptic astrocytic processes (PAPs)	Isolated astrocyte-GFP-tagged ribosome-bound RNA from the synaptoneurosome fraction from homogenized cortices (including hippocampi)	Soma and protrusion transcriptome and translatome	Mouse
Castro *et al.*, 2020	Perisynaptic Schwann Cells	Whole Perisynaptic Schwann Cells FACS sorted from P15-P21 S100β-GFP;NG2-dsRed mice	Whole FACS sorted PSCs	Mouse
Mazaré *et al.*, 2020	Perisynaptic astrocytic processes (PAPs)	Isolated astrocyte-GFP-tagged ribosome-bound RNA from synaptogliosomes from dorsal hippocampi	Soma and protrusion translatome	Mouse
Vasek *et al.*, 2021	Peripheral Microglia Processess (PEMPs)	GFP tagged ribosomes from Peripheral Microglia Processess	Protrusion translatome	Mouse

Table 4. A summary of all the available localized and synaptic glial transcriptomic datasets which were analyzed in this study. Most of the datasets explored transcripts localized to glial periphery, but the PSCs dataset was also included although it involved bulk transcriptomics because of its relevance to the glial involvement in synaptic plasticity.

These glial cell types include four studies of astrocytes, and one study each of oligodendrocytes, micro-dissected myelin and microglia. We also included one bulk transcriptomic study from Perisynaptic Schwann cells (PSCs) that are non-myelinating glia associated with the NMJ that were isolated from mice. We used the PSCs study because the isolated transcripts are associated with synapse activity, and therefore the dataset is highly relevant in our quest for mechanistic connections

between mRNA localization and synaptic plasticity (Castro *et al.*, 2020). The 8 studies used various methods of purifying localized transcripts, which are summarized in Table 4 “Specimen type” column, and in Figure 1A. We collated 8 transcriptomic and 4 TRAP (Translating Ribosome Affinity Purification) libraries, using a standardized pipeline for interoperability between the 12 datasets (Figure 1B). For details of how our analysis was performed and how we created a single data framework from all these independently acquired data sets, see the “Data meta-analysis methods” section of the “Materials and Methods”.

Using our bespoke data processing pipeline, we found 4,801 common transcripts detected in at least 8 libraries of localized mammalian glial transcripts. We tested whether this set of transcripts represents a population of localized mRNAs unique to the periphery of glia or whether they are also shared with the neurite transcriptome. To distinguish these possibilities, we compared the combined list of glial localized transcripts to the group of transcripts shown to commonly localize to the mammalian neuronal projections (von Kügelgen and Chekulaeva, 2020). We found a large overlap between the transcripts present at the periphery of both glia and neurons (Figure 1D). Our observations agree with a recent study highlighting conserved mRNA transport mechanisms between cell types (Goering, Arora and Taliaferro, 2022) and significant overlap of localized transcripts within astrocytes, radial glia and neurons (D'Arcy and Silver, 2020).

3.2 Meta-analysis of localized glial transcriptomes yields a predicted group of transcripts localized to the periphery of *Drosophila* peripheral glia

We then asked whether the mammalian glial localized transcripts were likely to be conserved across higher eukaryotes. To address this question in a specific case that is highly experimentally tractable, we intersected our mammalian dataset with the glial subtypes that extend their processes to the Peripheral Nervous System (PNS) of *Drosophila*, a well-established model for studying mRNA transport and local translation. We first filtered the 4,801 mammalian genes to only include the ones that have high confidence *Drosophila* homologues, retaining genes with a DIOPT score of at least 8 as a cutoff (Figure 1C). This filtering process resulted in a list of 3,513 *Drosophila* genes that we used to query the glial nuclear transcriptome from the Fly

Cell Atlas (Li *et al.*, 2022) (Figure 1E). We chose transcripts that were expressed in perineurial glia (PG) and subperineurial glia (SPG), the glial subtypes known to extend their processes to the *Drosophila* Neuromuscular Junction (NMJ) (Figure S1B and S1C). These glia have very long cytoplasmic extensions, and their cell bodies can be hundreds of micrometers away from their furthermost projections (Brink *et al.*, 2012a; Sepp, Schulte and Auld, 2000; Sepp, Schulte and Auld, 2001; Sepp and Auld, 2003) (Figure 1E). We also included ensheathing glia (EG), as they are the closest glial cell type in the Fly Cell Atlas that corresponds to wrapping glia (WG) of the PNS. The ensheathing glia in the CNS are continuous with the wrapping glia in the PNS, and express similar marker genes such as *nrv2* (Yildirim *et al.*, 2019) (Figure S1A). Our filtering of the mammalian glial localized mRNAs with high confidence *Drosophila* homologues by expression in any of the three *Drosophila* PNS glial subtypes (PG, SPG and WG/EG) yielded a group of 1,700 transcripts that we classify as “predicted to be present” in the projections of the *Drosophila* PNS glia. We hereafter refer to these transcripts as localized, in which we put emphasis on the presence of transcripts in the distal periphery rather than their enrichment compared with the cell body.

3.3 Gene ontology analysis reveals the statistical enrichment of transcripts related to mRNA trafficking, membrane composition and cytoskeletal regulation

To understand the functional characteristics of this group of localized transcripts, we identified enriched Gene Ontology (GO) terms followed by semantic similarity clustering of related terms within the localized 1,700 genes (Figure 2). Unclustered individual GO term enrichment results are given in Figure S2 and Supplementary Table 2. Our analysis revealed that the localized transcripts are enriched for biological processes involving morphogenesis/development, subcellular localization, cytoskeletal organization, signaling processes, and mRNA metabolism (Figure 2A). In terms of molecular function, RNA-binding, cytoskeleton-binding, as well as transmembrane transporter genes were highly enriched in our gene set (Figure 2B). Finally, our analysis of GO terms for the cellular component showed enrichment of terms related to vesicle/membrane transport, ribonucleoprotein granules and ribosomes in connection with the cytoskeleton, and the synapse, including synaptic

terminal, boutons and junctions (Figure 2C). Taken together, our GO enrichment analysis highlights statistically significant over-representation of functions related to membrane trafficking, cytoskeleton regulation, local translation, and cell-cell communication within the localized transcripts, all of which are likely to be very active at the distal periphery of polarized cells.

3.4 The 1,700 transcripts predicted to be present at the glial periphery are statistically enriched in neurodegenerative and neuropsychiatric disorders

Neurodegenerative and neuropsychiatric disorders have been associated with disruption of a number of post-transcriptional mechanisms, such as local translation, RNA-binding protein (RBP) activities and formation of RNA-rich granules (Blanco-Urrejola *et al.*, 2021). To determine whether our predicted *Drosophila* glial peripherally localized transcripts are statistically enriched in associations with previously studied nervous system disorders, we carried out a disease ontology enrichment analysis. We found a significant enrichment of disease terms related to neuropathologies in our set of 1,700 glial protrusion-localized transcripts (Figure 3A). Interestingly, terms related to neurodegeneration and dementia were particularly enriched in the 1,700 genes and were also found in previous studies to be connected to glial related mechanisms that cause the diseases (Blanco-Urrejola *et al.*, 2021). We also compared the set of 1,700 glial protrusion-localized transcripts with the SFARI gene database, which is a well-annotated list of genes that have associations with autism spectrum disorder (https://www.sfari.org/). We found a significant overlap between the 1,700 glial protrusion-localized transcripts and the SFARI genes (Figure 3B), further supporting the idea that mRNA localization in glia and the specific list of 1,700 genes we have highlighted are statistically enriched in genes associated with neurological disorders.

It was also very interesting to determine whether the 1,700 localized glial transcripts we highlighted are also enriched in signaling and enzymatic pathways. To investigate this possibility, we carried out a reactome-pathway enrichment analysis and found a significant enrichment of terms related to signaling pathways, such as Hedgehog or Wnt pathways, as well as terms related to mRNA translation, mRNA

stability regulation and nonsense-mediated decay (Figure 3C). These significant associations led us to hypothesize that many of the localized mRNAs at the periphery of glia are required for neuron-glia, glia-muscle or glia-glia communication, and localized mRNA processing and metabolism at the distal cytoplasm of glia. Such mechanisms could potentially include non-canonical mRNA processing that has been previously suggested to be involved in brain physiology and cancer (Pitolli *et al.*, 2022).

3.5 More than 70% of the previously identified glial transcripts are predicted to be present in the *Drosophila* PNS glia

Do the predicted transcripts indeed localize to the periphery of glial cells? To test our prediction in *Drosophila* glia, we cross-referenced the 1,700 transcripts against a list of 19 transcripts, which we previously identified experimentally to be present in the *Drosophila* peripheral glia by screening 200 randomly chosen genes for their localization status throughout the nervous system, including NMJ glia (Titlow *et al.*, 2022). We found that 15 out of 19 fly genes had high confidence mammalian homologues, so we carried out our comparison only with these 15 genes (see Table 5).

Found in Titlow et al.	FBgn ID	Is predicted in 1,700?
Lac	FBgn0010238	Yes
Pdi	FBgn0286818	Yes
nrv2	FBgn0015777	Yes
Lost	FBgn0263594	No
Flo-2	FBgn0264078	Yes
alpha-Cat	FBgn0010215	Yes
Vha55	FBgn0005671	Yes
Atpalpha	FBgn0002921	Yes
Nrg	FBgn0264975	Yes
Cip4	FBgn0035533	Yes
Nrx-IV	FBgn0013997	No
gs2	FBgn0001145	Yes
shot	FBgn0013733	Yes
kst	FBgn0004167	No
sdk	FBgn0021764	No

Table 5. A table indicating whether the 19 genes previously predicted to be present in the Drosophila glia have been predicted in the list of 1,700 Drosophila homologs. All transcripts which did not have a high confidence D. melanogaster orthologs of 4,801 genes that were detected in at least 8 datasets (DIOPT score ≥ 8) were removed.

We found that 11 out of the 15 transcripts (73.33%) were predicted from our analysis of mammalian glial transcripts to localize to the glial periphery in *Drosophila*. As these data originate from a systematic study of 200 mRNAs across the larval nervous system (Titlow *et al.*, 2022), we sought to repeat the experiments testing the localization status of the 11 genes in greater detail, using smFISH together with markers of specific glial sub-types (Figure 4 and S4, see “Experimental methods” for details). Our results confirmed with greater confidence that all 11 transcripts were indeed present in the peripheral glia at the *Drosophila* NMJ. To determine the statistical significance of the 11/15 hits, we carried out an enrichment test that follows a hypergeometric distribution (independent sampling). Our results showed a slim probability of 8.37×10^{-05} for the 73% overlap to have occurred by chance, hence assuming a significant over-representation. We conclude that the predicted group of 1,700 are highly likely to be peripherally localised in *Drosophila* cytoplasmic glial projections.

Our secondary analysis also allowed us to obtain higher resolution single mRNA molecule information on the distributions of mRNAs molecules across the motoneuron axons and the surrounding glial protrusions (Figure 4 and Figure S4). We found specific examples of transcripts that were highly enriched in glia, with a much lower abundance in the motoneurons, including *gs2*, *nrv2*, *flo-2* and *Lac* (Figure 4 and S4A, B, G respectively). Other transcripts were uniformly distributed in motoneurons, glia and muscle cells in the NMJ, including *Cip4*, *Pdi*, *Vha55*, *Nrg*, *alpha-Cat*, *Atpalpha*, *shot* (Figure S4, C-F, H-J, respectively). In conclusion, these results show that the localization of transcripts, extrapolated from vertebrates to *Drosophila,* were highly concordant, reliably predicting the presence of multiple mRNAs at the glial periphery and highlighting a possible evolutionary conservation of glial protrusion-localized transcriptome.

3.6 Localized glial transcripts influence plasticity in the adjacent motoneurons

To test the function of the glial localized mRNAs to influence synaptic plasticity of the neighboring motoneurons, we knocked down the genes specifically in glia, with the motoneurons remaining unaffected. We used 13 UAS-RNAi lines (against 11

different transcripts) driven by the pan-glial Repo-GAL4 driver (see materials and methods for further details). We assayed the impact of knocking down each gene in glia on the ability of the wild type NMJ motoneurons to make new synapses in response to chemical stimulation of the nerve. We applied the well-established protocol for activity-dependent synaptic plasticity through spaced pulses of potassium applied to a living NMJ preparation (Ataman *et al.*, 2008; Roche *et al.*, 2002; Piccioli and Littleton, 2014; Vasin *et al.*, 2014). We found that 10 of the UAS-RNAi lines were viable until 3rd instar larvae without causing excessive lethality. RNAi knockdown of *Cip4* in glia did not yield viable 3rd instar larvae, so this gene was excluded from further analysis. Therefore, we tested 10 out of 11 localized transcripts in glia for their involvement in regulating synaptic plasticity of motoneurons. Interestingly, we found that Repo>*Vha55*-RNAi larvae display a small central brain phenotype (Figure S5), however the larvae were otherwise indistinguishable in size from their control counterparts, so they were assayed as with other genotypes.

We performed the spaced potassium stimulation assay (Figure 5A) to quantitate the effect of glial-specific RNAi by counting the number of newly formed neuronal boutons defined as “ghost” boutons, which are immature structures that lack post-synaptic density markers such as Discs large 1 (*Dlg1*) protein (Ataman *et al.*, 2008; Roche *et al.*, 2002). We found that for 3 of the 10 transcripts (*Lac*, *gs2*, *Pdi*) the RNAi knockdown in *Drosophila* glia causes a reduction in the number of ghost boutons formed in response to pulses of potassium (Figure 5B, C). We conclude that *Lac*, *gs2* and *Pdi* are required within glia for the correct plasticity of the motoneuron synapses.

We also assayed the effect of knocking down the localized transcripts in glia on the morphology of the glial projections and of the wild-type axon terminals in the NMJ. We examined the morphologies of 3rd instar glia expressing RNAi and wild type motoneurons (Figure 5 D, E) with or without potassium stimulation (Figure 5 F, G). We found that, even in the absence of stimulation, the knock-down of many of the genes resulted in aberrant growth or shrinkage of glial projections as well as a change in the ratio of glial to neuron surface areas, suggesting a developmental defect. For example, RNAi against *shot* resulted in near elimination of the glial projections. While in the control larvae, the glial projections extend on the surface of

the muscle cells, in *shot*-RNAi larvae the non-synaptic motor axon branches are covered with glia, but the glia lack any projections onto the surface of the muscle (Figure 5D, E). We also saw varying defects in the sizes of both glial and neuronal projections after spaced potassium stimulation (Figure 5F, G). Our results demonstrate that many of the localized glial transcripts are required for the correct morphology of the *Drosophila* NMJ, and 30% are specifically necessary in glia for the correct synaptic plasticity of their neighboring neuron.

4 Discussion

4.1 Transcripts localized to the projections of different glial subtypes have conserved roles in coordinating synaptic plasticity and development

Using meta-analysis of multiple published datasets of peripherally localized mammalian glial mRNAs, we have predicted 1,700 localized transcripts in 3 glial subtypes associated with the *Drosophila* motoneurons and NMJ synapses. These mRNAs are highly enriched in *Drosophila* homologues of human genes with associations in a variety of neurodegenerative and neuropsychiatric diseases, which also often coincide with molecular and cellular functions that have known associations with the cell periphery (Figure 1). The localized glial mRNA we predict include regulators of cytoskeleton dynamics and remodeling, membrane dynamics, signaling pathways and mRNA metabolism (Figure 2). We tested some of these predictions by using smFISH to characterize in more detail the localization of 15 out of 19 of the mRNAs that we previously identified as present in *Drosophila* glia (Titlow *et al.*, 2022) and possessing high confidence mammalian homologues. We found that 11 out of the 15 predicted transcripts were indeed localized in the glial periphery near the NMJ, suggesting that our meta-analysis holds strong predictive value, given that the probability of this happening by chance is ~10^{-5} (Figure 3). Moreover, we found that in three cases (*Lac*, *gs2*, and *Pdi*), the localized transcripts are specifically required in glia for the correct synaptic plasticity in the adjacent motoneurons.

Knock-down of glial localized transcripts also causes morphological defects in the synapse (Figure 5). Interestingly, morphological effects were not always associated

with defects in activity-dependent plasticity, and were also not always cell autonomous. These results highlight the complexity of intercellular communication necessary for proper synapse development and function. We conclude that our group of 1,700 mRNAs predicted to localize in *Drosophila* glia adjacent to the NMJ are likely to represent a rich resource of functionally relevant transcripts, which in many cases have associations with neurodegenerative, neuropsychiatric and other important nervous system diseases, further emphasizing the power of data interoperability in biological research.

It is important to consider whether the 1,700 transcripts that we predict are localized in the three glial sub-types associated with the NMJ, are in fact a core localized glial transcriptome that is functionally active in the protrusions of any glial cell type. Certainly, the glial sub-types we characterized in *Drosophila* at the NMJ are also present, as defined by specific cell type markers, in association with neurons and synapses in the central brain. Furthermore, recent studies suggest that mRNA localization in one cell type mediated by interactions with RBPs can be predictive of the same interactions and localizations in other cell types with very different morphologies and functions (Goering, Arora and Taliaferro, 2022). It has also been shown that radial glia, astrocytes, and neurons, all of which have quite distinct morphologies and functions, share a significant overlap in the types of mRNAs localized to their protrusions (D'Arcy and Silver, 2020). Perhaps cytoplasmic peripheries of any kind of cell type share many universal properties in common, such as membrane trafficking and cytoskeletal dynamics.

4.2 Glial protrusion transcriptomes contain a significant enrichment of disease ontology terms related to neuropathologies

Our analysis has indicated a significant enrichment of terms related to associations with nervous system diseases among the 1,700 *Drosophila* homologues with predicted glial mRNA localization (Figure 3). Moreover, this group of genes has a statistically significant overlap with the SFARI database, which contains a list of genes implicated in Autism Spectrum Disorder (ASD). There is a growing interest in the role that glial cells may play in the mechanistic causes of diverse diseases

related to nervous system development and function. Indeed, it has been suggested that mRNA localization and local translation could cause glial-induced pathological effects (Sloan and Barres, 2013; Prater, Latimer and Jayadev, 2022). Our results bolster this idea and the dearth of literature in this area only serves to emphasize the need for more experimental work with a holistic approach to the nervous system, including glia and their communication with neurons at tripartite synapses. Although aggregated research made available in databases like SFARI mostly focuses on neuronal studies (Banerjee-Basu and Packer, 2010), our work shows that many SFARI genes are transcribed into mRNA that is localized to glial protrusions. We have also shown that the reactome-pathway analysis of glial localized transcripts uncovers many enriched terms related both to signaling and mRNA metabolism, providing hints at potential unexplored mechanisms related to nervous system disorders. Another highly enriched reactome pathway term worth highlighting is the “innate immune system”, which indicates that the availability of gene lists like ours is potentially valuable for multiple fields of research, as they extend beyond the context of the nervous system. Analysis modes like ours could prove useful in predicting which mRNAs might be localized in immune cells based on whether they are found in neurites.

An important direction of future research will be to characterize local translation at the peripheral cytoplasm of glia in response to signaling and neuronal activity, as was done in one recent study, which we included in our meta-analysis (Mazaré *et al.*, 2020). The *Drosophila* larval system is a particularly good experimental system to study glia in relation to plasticity, because of the ease of access to the NMJ and the ability to precisely assay the role of glia in the plasticity of the motoneurons. Moreover, the extensive genetic toolbox available in *Drosophila* makes the model very tractable and well suited to studying the mechanistic effects of the introduction of disease mutations specifically into synaptic glia.

4.3 Vertebrate localization data meta-analysis correctly predicts mRNA localization for the majority of transcripts

Using smFISH we confirmed, with greater precision, the presence of 11 transcripts of interest in *Drosophila* glial projections, which we had discovered in a recent survey of

200 transcripts across the larval nervous system (Titlow *et al.*, 2022). We have focused on the glial cell subtypes that reach the *Drosophila* NMJ because of their extensive morphologies and close contacts with the NMJ synapses (Figure S1). The NMJ associated glial subtypes are also present in the central brain, but unlike in the larval brain, in the NMJ the individual glial projections can be observed under the microscope together with individual synapses. Building on our prior work (Titlow *et al.*, 2022), we confirmed that the mammalian localization data, which we re-analysed and intersected with *Drosophila* glia, correctly predicts glial mRNA localization in *Drosophila*. We conclude that peripheral glial mRNA localization is a common and conserved phenomenon and propose that it is therefore likely to be functionally important. Naturally our work is limited by the number of transcripts that could be tested experimentally. In the future, it will be important to continue to explore the localization of many more of the 1,700 *Drosophila* transcripts and test their functional requirement in glia as well as their potential implications for novel mechanisms of diseases of the nervous system.

5 Contributions, conflict of interest, funding details

Author contributions:

Dalia S. Gala: Conceptualization, Methodology, Validation, Formal analysis, Investigation, Data Curation, Writing - Original Draft, Writing - Review & Editing, Visualization. **Jeffrey Y. Lee:** Conceptualization, Methodology, Software, Validation, Formal analysis, Resources, Data Curation, Writing - Review & Editing, Visualization. **Maria Kiourlappou:** Methodology, Software, Formal analysis, Data Curation, Writing - Review & Editing. **Joshua S. Titlow:** Conceptualization, Methodology, Writing - Review & Editing, Supervision. **Rita O. Teodoro**: Methodology, Resources, Writing - Review & Editing, Supervision. **Ilan Davis:** Conceptualization, Resources, Writing - Original Draft, Writing - Review & Editing, Supervision, Project administration, Funding acquisition.

Conflicts of Interest:

The authors declare no competing or financial interests.

Funding statement:

This work was funded by a Wellcome Investigator Award 209412/Z/17/Z and Wellcome Strategic Awards (Micron Oxford) 091911/B/10/Z and 107457/Z/15/Z to I.D. M.K. was supported by the Biotechnology and Biosciences Research Council (BBSRC), grant numbers: (BB/M011224/1) and (BB/S507623/1). D.S.G. is funded by Medial Sciences Graduate Studentships, University of Oxford. R.O.T. is funded by iNOVA4Health – UIDB/04462/2020 and EXPL/BIA-CEL/1484/2021.

6 References

Abràmoff, M. D., Magalhães, P. J. and Ram, S. J. (2004) 'Image processing with ImageJ', *Biophotonics international,* 11(7), pp. 36-42.

Alexa, A. and Rahnenfuhrer, J. 2022. *topGO: Enrichment Analysis for Gene Ontology*. R package version 2.48.0. ed.

Allen, N. J. and Lyons, D. A. (2018) 'Glia as architects of central nervous system formation and function', *Science,* 362(6411), pp. 181-185.

Andoh, M. and Koyama, R. (2021) 'Microglia regulate synaptic development and plasticity', *Developmental Neurobiology,* 81(5), pp. 568-590.

Ataman, B., Ashley, J., Gorczyca, M., Ramachandran, P., Fouquet, W., Sigrist, S. J. and Budnik, V. (2008) 'Rapid Activity-Dependent Modifications in Synaptic Structure and Function Require Bidirectional Wnt Signaling', *Neuron*.

Azevedo, M. M., Domingues, H. S., Cordelières, F. P., Sampaio, P., Seixas, A. I. and Relvas, J. B. (2018) 'Jmy regulates oligodendrocyte differentiation via modulation of actin cytoskeleton dynamics', *GLIA*.

Bacmeister, C. M., Barr, H. J., McClain, C. R., Thornton, M. A., Nettles, D., Welle, C. G. and Hughes, E. G. (2020) 'Motor learning promotes remyelination via new and surviving oligodendrocytes', *Nat Neurosci,* 23(7), pp. 819-831.

Banerjee-Basu, S. and Packer, A. (2010) 'SFARI Gene: an evolving database for the autism research community', *Dis Model Mech,* 3(3-4), pp. 133-5.

Biever, A., Donlin-Asp, P. G. and Schuman, E. M. (2019) 'Local translation in neuronal processes', *Current Opinion in Neurobiology,* 57, pp. 141-148.

Blanco-Urrejola, M., Gaminde-Blasco, A., Gamarra, M., de la Cruz, A., Vecino, E., Alberdi, E. and Baleriola, J. (2021) 'RNA Localization and Local Translation in Glia in Neurological and Neurodegenerative Diseases: Lessons from Neurons', *Cells*.

Boulay, A. C., Saubameá, B., Adam, N., Chasseigneaux, S., Mazaré, N., Gilbert, A., Bahin, M., Bastianelli, L., Blugeon, C., Perrin, S., Pouch, J., Ducos, B., Le Crom, S., Genovesio, A., Chrétien, F., Declèves, X., Laplanche, J. L. and Cohen-Salmon, M. (2017) 'Translation in astrocyte distal processes sets molecular heterogeneity at the gliovascular interface', *Cell Discovery,* 3.

Bray, N. L., Pimentel, H., Melsted, P. and Pachter, L. (2016) 'Near-optimal probabilistic RNA-seq quantification', *Nature Biotechnology,* 34(5), pp. 525-527.

Brink, D. L., Gilbert, M., Xie, X., Petley-Ragan, L. and Auld, V. J. (2012a) 'Glial processes at the Drosophila larval neuromuscular junction match synaptic growth', *PLoS ONE*.

Brink, D. L., Gilbert, M., Xie, X., Petley-Ragan, L. and Auld, V. J. (2012b) 'Glial processes at the Drosophila larval neuromuscular junction match synaptic growth', *PLoS One,* 7(5), pp. e37876.

Bushnell, B., Rood, J. and Singer, E. (2017) 'BBMerge – Accurate paired shotgun read merging via overlap', *PLOS ONE,* 12(10), pp. e0185056.

Castro, R., Taetzsch, T., Vaughan, S. K., Godbe, K., Chappell, J., Settlage, R. E. and Valdez, G. (2020) 'Specific labeling of synaptic schwann cells reveals unique cellular and molecular features', *eLife*.

D'Arcy, B. R. and Silver, D. L. (2020) 'Local gene regulation in radial glia: Lessons from across the nervous system', *Traffic,* 21(12), pp. 737-748.

Daniel E Shumer, N. J. N. N. P. S. (2017) '乳鼠心肌提取 HHS Public Access', *Physiology & behavior,* 176(12), pp. 139-148.

de Faria, O., Pivonkova, H., Varga, B., Timmler, S., Evans, K. A. and Káradóttir, R. T. (2021) 'Periods of synchronized myelin changes shape brain function and plasticity', *Nat Neurosci,* 24(11), pp. 1508-1521.

De Pittà, M., Brunel, N. and Volterra, A. (2016) 'Astrocytes: Orchestrating synaptic plasticity?', *Neuroscience,* 323, pp. 43-61.

Fields, R. D. (2005) 'Myelination: An overlooked mechanism of synaptic plasticity?', *Neuroscientist,* 11(6), pp. 528-531.

Fields, R. D. (2008) 'Oligodendrocytes changing the rules: action potentials in glia and oligodendrocytes controlling action potentials', *Neuroscientist,* 14(6), pp. 540-3.

Fields, R. D. and Bukalo, O. (2020) 'Myelin makes memories', *Nat Neurosci,* 23(4), pp. 469-470.

Goering, R., Arora, A. and Taliaferro, J. M. (2022) 'RNA localization mechanisms transcend cell morphology', *bioRxiv*, pp. 2022.04.14.488401.

Graeber, M. B. (2010) 'Changing face of microglia', *Science,* 330(6005), pp. 783-8.

Gu, Z. and Hübschmann, D. (2022) 'Simplify enrichment: A bioconductor package for clustering and visualizing functional enrichment results', *Genomics Proteomics Bioinformatics*.

Holt, C. E., Martin, K. C. and Schuman, E. M. (2019) 'Local translation in neurons: visualization and function', *Nature Structural and Molecular Biology,* 26(7), pp. 557-566.

Hu, Y., Flockhart, I., Vinayagam, A., Bergwitz, C., Berger, B., Perrimon, N. and Mohr, S. E. (2011) 'An integrative approach to ortholog prediction for disease-focused and other functional studies', *BMC Bioinformatics,* 12, pp. 357.

Ignatiadis, N., Klaus, B., Zaugg, J. B. and Huber, W. (2016) 'Data-driven hypothesis weighting increases detection power in genome-scale multiple testing', *Nature Methods,* 13(7), pp. 577-580.

Jessen, K. R., Mirsky, R. and Lloyd, A. C. (2015) 'Schwann cells: Development and role in nerve repair', *Cold Spring Harbor Perspectives in Biology,* 7(7), pp. 1-15.

Li, H. and Janssens, J. and De Waegeneer, M. and Kolluru, S. S. and Davie, K. and Gardeux, V. and Saelens, W. and David, F. P. A. and Brbić, M. and Spanier, K. and Leskovec, J. and

McLaughlin, C. N. and Xie, Q. and Jones, R. C. and Brueckner, K. and Shim, J. and Tattikota, S. G. and Schnorrer, F. and Rust, K. and Nystul, T. G. and Carvalho-Santos, Z. and Ribeiro, C. and Pal, S. and Mahadevaraju, S. and Przytycka, T. M. and Allen, A. M. and Goodwin, S. F. and Berry, C. W. and Fuller, M. T. and White-Cooper, H. and Matunis, E. L. and DiNardo, S. and Galenza, A. and O'Brien, L. E. and Dow, J. A. T. and Jasper, H. and Oliver, B. and Perrimon, N. and Deplancke, B. and Quake, S. R. and Luo, L. and Aerts, S. and Agarwal, D. and Ahmed-Braimah, Y. and Arbeitman, M. and Ariss, M. M. and Augsburger, J. and Ayush, K. and Baker, C. C. and Banisch, T. and Birker, K. and Bodmer, R. and Bolival, B. and Brantley, S. E. and Brill, J. A. and Brown, N. C. and Buehner, N. A. and Cai, X. T. and Cardoso-Figueiredo, R. and Casares, F. and Chang, A. and Clandinin, T. R. and Crasta, S. and Desplan, C. and Detweiler, A. M. and Dhakan, D. B. and Donà, E. and Engert, S. and Floc'hlay, S. and George, N. and González-Segarra, A. J. and Groves, A. K. and Gumbin, S. and Guo, Y. and Harris, D. E. and Heifetz, Y. and Holtz, S. L. and Horns, F. and Hudry, B. and Hung, R. J. and Jan, Y. N. and Jaszczak, J. S. and Jefferis, G. S. X. E. and Karkanias, J. and Karr, T. L. and Katheder, N. S. and Kezos, J. and Kim, A. A. and Kim, S. K. and Kockel, L. and Konstantinides, N. and Kornberg, T. B. and Krause, H. M. and Labott, A. T. and Laturney, M. and Lehmann, R. and Leinwand, S. and Li, J. and Li, J. S. S. and Li, K. and Li, L. and Li, T. and Litovchenko, M. and Liu, H. H. and Liu, Y. and Lu, T. C. and Manning, J. and Mase, A. and Matera-Vatnick, M. and Matias, N. R. and McDonough-Goldstein, C. E. and McGeever, A. and McLachlan, A. D. and Moreno-Roman, P. and Neff, N. and Neville, M. and Ngo, S. and Nielsen, T. and O'Brien, C. E. and Osumi-Sutherland, D. and Özel, M. N. and Papatheodorou, I. and Petkovic, M. and Pilgrim, C. and Pisco, A. O. and Reisenman, C. and Sanders, E. N. and Dos Santos, G. and Scott, K. and Sherlekar, A. and Shiu, P. and Sims, D. and Sit, R. V. and Slaidina, M. and Smith, H. E. and Sterne, G. and Su, Y. H. and Sutton, D. and Tamayo, M. and Tan, M. and Tastekin, I. and Treiber, C. and Vacek, D. and Vogler, G. and Waddell, S. and Wang, W. and Wilson, R. I. and Wolfner, M. F. and Wong, Y. E. and Xie, A. and Xu, J. and Yamamoto, S. and Yan, J. and Yao, Z. and Yoda, K. and Zhu, R. and Zinzen, R. P. and Consortium§, F. (2022) 'Fly Cell Atlas: A single-nucleus transcriptomic atlas of the adult fruit fly', *Science,* 375(6584), pp. eabk2432.

Love, M. I., Huber, W. and Anders, S. (2014) 'Moderated estimation of fold change and dispersion for RNA-seq data with DESeq2', *Genome Biology,* 15(12), pp. 550.

Mazaré, N., Oudart, M., Moulard, J., Cheung, G., Tortuyaux, R., Mailly, P., Mazaud, D., Bemelmans, A. P., Boulay, A. C., Blugeon, C., Jourdren, L., Le Crom, S., Rouach, N. and Cohen-Salmon, M. (2020) 'Local Translation in Perisynaptic Astrocytic Processes Is Specific and Changes after Fear Conditioning', *Cell Reports*.

Melsted, P., Booeshaghi, A. S., Liu, L., Gao, F., Lu, L., Min, K. H., da Veiga Beltrame, E., Hjörleifsson, K. E., Gehring, J. and Pachter, L. (2021) 'Modular, efficient and constant-memory single-cell RNA-seq preprocessing', *Nature Biotechnology,* 39(7), pp. 813-818.

Meservey, L. M., Topkar, V. V. and Fu, M. m. (2021) 'mRNA Transport and Local Translation in Glia', *Trends in Cell Biology,* 31(6), pp. 419-423.

Morris, G. P., Clark, I. A., Zinn, R. and Vissel, B. (2013) 'Microglia: A new frontier for synaptic plasticity, learning and memory, and neurodegenerative disease research', *Neurobiology of Learning and Memory,* 105, pp. 40-53.

Ota, Y., Zanetti, A. T. and Hallock, R. M. (2013) 'The role of astrocytes in the regulation of synaptic plasticity and memory formation', *Neural Plast,* 2013, pp. 185463.

Pan, S., Mayoral, S. R., Choi, H. S., Chan, J. R. and Kheirbek, M. A. (2020) 'Preservation of a remote fear memory requires new myelin formation', *Nat Neurosci,* 23(4), pp. 487-499.

Piccioli, Z. D. and Littleton, J. T. (2014) 'Retrograde BMP signaling modulates rapid activity-dependent synaptic growth via presynaptic LIM kinase regulation of cofilin', *J Neurosci,* 34(12), pp. 4371-81.

Pitolli, C., Marini, A., Sette, C. and Pagliarini, V. (2022) 'Non-Canonical Splicing and Its Implications in Brain Physiology and Cancer', *Int J Mol Sci,* 23(5).

Prater, K. E., Latimer, C. S. and Jayadev, S. (2022) 'Glial TDP-43 and TDP-43 induced glial pathology, focus on neurodegenerative proteinopathy syndromes', *Glia,* 70(2), pp. 239-255.

Rangaraju, V., tom Dieck, S. and Schuman, E. M. (2017) 'Local translation in neuronal compartments: how local is local?', *EMBO reports,* 18(5), pp. 693-711.

Ransom, B. R. and Ransom, C. B. (2012) *Astrocytes: Multitalented stars of the central nervous system.*

Roche, J. P., Packard, M. C., Moeckel-Cole, S. and Budnik, V. (2002) 'Regulation of synaptic plasticity and synaptic vesicle dynamics by the PDZ protein scribble', *Journal of Neuroscience*.

Sakers, K., Lake, A. M., Khazanchi, R., Ouwenga, R., Vasek, M. J., Dani, A. and Dougherty, J. D. (2017) 'Astrocytes locally translate transcripts in their peripheral processes', *Proceedings of the National Academy of Sciences of the United States of America,* 114(19), pp. E3830-E3838.

Schafer, D. P., Lehrman, E. K., Kautzman, A. G., Koyama, R., Mardinly, A. R., Yamasaki, R., Ransohoff, R. M., Greenberg, M. E., Barres, B. A. and Stevens, B. (2012) 'Microglia sculpt postnatal neural circuits in an activity and complement-dependent manner', *Neuron,* 74(4), pp. 691-705.

Schneider, C. A., Rasband, W. S. and Eliceiri, K. W. (2012) 'NIH Image to ImageJ: 25 years of image analysis', *Nat Methods,* 9(7), pp. 671-5.

Sepp, K. J. and Auld, V. J. (2003) 'Reciprocal Interactions between Neurons and Glia Are Required for', *Cell,* 23(23), pp. 8221-8230.

Sepp, K. J., Schulte, J. and Auld, V. J. (2000) 'Developmental dynamics of peripheral glia in Drosophila melanogaster', *Glia,* 30(2), pp. 122-133.

Sepp, K. J., Schulte, J. and Auld, V. J. (2001) 'Peripheral glia direct axon guidance across the CNS/PNS transition zone', *Developmental Biology,* 238(1), pp. 47-63.

Sloan, S. A. and Barres, B. A. (2013) 'Glia as primary drivers of neuropathology in TDP-43 proteinopathies', *Proc Natl Acad Sci U S A,* 110(12), pp. 4439-40.

Smith, W. B., Aakalu, G. and Schuman, E. M. (2001) 'Local protein synthesis in neurons Girish Aakalu and', *Current Biology*, pp. 901-903.

Sutton, M. A. and Schuman, E. M. (2006) 'Dendritic Protein Synthesis, Synaptic Plasticity, and Memory', *Cell,* 127(1), pp. 49-58.

Terenzio, M., Schiavo, G. and Fainzilber, M. (2017) 'Compartmentalized Signaling in Neurons: From Cell Biology to Neuroscience', *Neuron,* 96(3), pp. 667-679.

Thakurela, S., Garding, A., Jung, R. B., Müller, C., Goebbels, S., White, R., Werner, H. B. and Tiwari, V. K. (2016) 'The transcriptome of mouse central nervous system myelin', *Scientific Reports*.

Thomsen, R., Pallesen, J., Daugaard, T. F., Børglum, A. D. and Nielsen, A. L. (2013) 'Genome wide assessment of mRNA in astrocyte protrusions by direct RNA sequencing reveals mRNA localization for the intermediate filament protein nestin', *Glia,* 61(11), pp. 1922-1937.

Titlow, J. S., Kiourlappou, M., Palanca, A., Lee, J. Y., Gala, D. S., Ennis, D., Yu, J. J. S., Young, F. L., Susano Pinto, D. M., Garforth, S., Francis, H. S., Strivens, F., Mulvey, H., Dallman-Porter, A.,

Thornton, S., Arman, D., Järvelin, A. I., Thompson, M. K., Kounatidis, I., Parton, R. M., Taylor, S. and Davis, I. (2022) 'Systematic analysis of YFP gene traps reveals common discordance between mRNA and protein across the nervous system', *bioRxiv*, pp. 2022.03.21.485142.

Vasek, M. J., Deajon-jackson, J. D., Liu, Y., Crosby, H. W. and Mo, S. L. (2021) 'Microglia perform local protein synthesis at perisynaptic and phagocytic structures Affiliations : Department of Genetics , Washington University School of Medicine , 660 S . Euclid Ave , Department of Psychiatry , Washington University School of Medicine'.

Vasin, A., Zueva, L., Torrez, C., Volfson, D., Littleton, J. T. and Bykhovskaia, M. (2014) 'Synapsin regulates activity-dependent outgrowth of synaptic boutons at the Drosophila neuromuscular junction', *J Neurosci,* 34(32), pp. 10554-63.

Volterra, A. and Meldolesi, J. (2005) 'Astrocytes, from brain glue to communication elements: the revolution continues', *Nature Reviews Neuroscience,* 6(8), pp. 626-640.

von Kügelgen, N. and Chekulaeva, M. 2020. Conservation of a core neurite transcriptome across neuronal types and species.

Wang, D. O., Kim, S. M., Zhao, Y., Hwang, H., Miura, S. K., Sossin, W. S. and Martin, K. C. (2009) 'Synapse- and stimulus-specific local translation during long-term neuronal plasticity', *Science,* 324(5934), pp. 1536-40.

Wang, D. O., Martin, K. C. and Zukin, R. S. (2010) 'Spatially restricting gene expression by local translation at synapses', *Trends in Neurosciences,* 33(4), pp. 173-182.

Wang, Y., Fu, A. K. Y. and Ip, N. Y. (2022) 'Instructive roles of astrocytes in hippocampal synaptic plasticity: neuronal activity-dependent regulatory mechanisms', *FEBS J,* 289(8), pp. 2202-2218.

Xie, X. and Auld, V. J. (2011) 'Integrins are necessary for the development and maintenance of the glial layers in the Drosophila peripheral nerve', *Development,* 138(17), pp. 3813-22.

Yildirim, K., Petri, J., Kottmeier, R. and Klämbt, C. (2019) 'Drosophila glia: Few cell types and many conserved functions', *Glia,* 67(1), pp. 5-26.

7 Figure legends

Figure 1. Conserved transcripts localized to glial protrusions. A) A graphical representation of the techniques used to separate the protrusion-localized transcripts in each study, with the exception of PSCs (middle), where whole cells were used. B) Bar graph showing the datasets included in this study. High confidence expression cut-off was set at TPM > 10, and transcripts detected in more than 3 independent datasets are shown in orange color. C) Identification of high confidence *D. melanogaster* orthologs of 4,801 genes that were detected in at least 8 datasets. DRSC Integrative Ortholog Prediction Tool (DIOPT) score of 8 was used as cut-off. D) Comparison of transcripts localized, enriched or translated in the glial protrusion and/or neurites (von Kügelgen and Chekulaeva, 2020). Transcripts were considered

enriched when log2FoldChange > 0 and adjusted p-value < 0.05, comparing protrusion and soma compartment-specific RNA-seq libraries. TRAP-seq TPM > 10 was considered as existence of translation. E) t-SNE plot of combined glial single-nuclei RNA-seq from the Fly Cell Atlas (Li *et al.*, 2022). Perineurial, subperineurial and ensheathing glial cell clusters are depicted in orange-red colors. F) A schematic representing the distribution and location of glial cells in the *Drosophila* 3rd instar larva. Six subtypes of glia exist in the larvae: perineurial and subperineurial glia, cortex glia, astrocyte-like and ensheathing glial cells and, finally, the peripheral nervous system (PNS) specific wrapping glia (Yildirim *et al.*, 2019). Ensheathing glia of the CNS are continuous with the wrapping glia of the CNS. The perineurial and subperineurial glia have long and extensive projections which reach all the way to the neuromuscular junction (NMJ).

Figure S1. Confocal images of *Drosophila* peripheral glia. Confocal images representing the location of **A)** wrapping glia (*nrv2*-GAL4), **B)** subperineurial glia (Mdr65-GAL4) and **C)** perineurial glia (46F-GAL4) in the *Drosophila* 3rd instar larva. All three of these glial subtypes produce extensive projections which reach hundreds of microns away from the cell body and reach the neuromuscular junction (NMJ) (middle two panels of each section). These three glial cell subtypes were chosen in our filtering for their elongated morphologies and the direct microscopically observable contact with the NMJ synapse. For each of A), B) and C): **i)** represents the 10x overview of the whole dissected larva, **ii)** represents a 40x zoom of segments A2 and A3 of muscles 6/7. **iii)** presents an overview of the NMJ, and **iv)** is a zoomed-in section of each of the images in **iii)**, as indicated by the white boxes. **v)** and **vi)** show the individual channels from **iv)** for clarity, with the channel label specified in the top left corner of **v)** - glia and **vi)** – anti-HRP.

Figure 2 Functional annotation of glial protrusion-localized transcripts. A-C) Overviews of gene ontology (GO) terms enriched in the 1,700 glial protrusion-localized transcripts Biological Process, Molecular Function and Cellular Component categories. Enriched GO terms (FoldChange > 1.5, adjusted p-value < 0.01) were clustered based on the semantic similarity. Word clouds for each cluster show over-

represented terms. *D. melanogaster* genes with high-confidence orthologues to *M. musculus* genes (DIOPT score ≥ 8) were used as background.

Figure S2. Enriched gene ontology (GO) terms of glial protrusion-localized transcripts. A-C) Volcano plot of GO terms enriched in the 1,700 glial protrusion-localized transcripts in Biological Process, Molecular Function and Cellular Component categories. *D. melanogaster* genes with high-confidence orthologues to *M. musculus* genes (DIOPT score ≥ 8) were used as background. Full GO enrichment analysis table is given in Supplementary Table 2.

Figure 3. Association of glial protrusion-localized transcripts with disease. A) Enrichment of disease ontology (DO) terms in the 1,700 glial protrusion-localized transcripts. DO terms from *D. melanogaster* genes with high-confidence orthologues to *M. musculus* genes (DIOPT score ≥ 8) were used as background. Enrichment was assessed with hypergeometric test and corrected for multiple hypothesis testing. **B)** Significant overlap between the 1,700 glial protrusion-localized transcripts and the SFARI list of genes. SFARI gene is an annotated list of genes that have been investigated in the context of autism spectrum disorder (Banerjee-Basu and Packer, 2010). 1,095 *H. sapiens* SFARI genes were converted to *D. melanogaster* genes (DIOPT score ≥ 8) before the statistical enrichment. **C)** Reactome pathway enrichment analysis of the 1,700 glial protrusion-localized transcripts against the whole D. Melanogaster genome as background. The size of the of the points shows the number of localized genes corresponding to the term and the color of the point indicates the parent term in the Reactome pathways hierarchy. Enrichment was assessed with hypergeometric test and corrected for multiple hypothesis testing.

Figure 4. Localization of *gs2*::YFP transcripts in *Drosophila* glia. A) A confocal image of the *Drosophila* 3rd instar larva NMJ (Segment A4), showing the neuron and muscle cell nuclei in blue (anti-HRP antibody conjugated to Alexa-405 fluor and DAPI, respectively), *gs2*::YFP protein in green, glial membrane of perisynaptic glia labelled with Repo>mCD8-mCherry in magenta, and the YFP exon associated with *gs2*::YFP protein in white (Atto-633). **B-D)** A single-channel view (see label) of a

zoomed-in area **i)** of A) in which multiple mRNA molecules are present in the glial projection. **E)** A zoomed in area **ii)** of A) showing the entire length of the perisynaptic glia at that synapse with the mRNA molecules distributed regularly throughout the glial cell projections.

Figure S4. Localization of predicted transcripts in *Drosophila* glia. B-K) Confocal images of the *Drosophila* 3rd instar larva NMJs (Segments A3 or A4), showing the **i)** neuron and muscle cell nuclei in blue (anti-HRP antibody conjugated to Alexa-405 fluor and DAPI, respectively), YFP conjugated proteins in green (see in-image label for details), glial membrane of perisynaptic glia labelled with Repo>mCD8-mCherry in magenta, and the YFP exon associated with the protein in white (Atto-633). For all transcripts, mRNA was detected within glial membrane labelling, as indicated in **ii)** for each panel, where a zoomed in area denoted by a white rectangle in i) is presented.

Figure 5. Knockdown of glial localized transcripts interferes with synaptic plasticity and development. A) A schematic representation of the spaced potassium stimulation assay used in this study. Larvae are dissected and subjected to pulses of high potassium solution mimicking neuromuscular stimulation. After the assay has been completed, newly formed axon terminal endings with immature synapses, called “ghost boutons”, can be detected using anti-HRP antibody labelling thanks to the lack of the post-synaptic density present, which can be labelled using anti-Discs-large antibody, which the ghost boutons lack. **B)** Knock-downs of multiple glial protrusion-localized transcripts disrupt synaptic plasticity. Bar graph represents average log2 FoldChange of bouton counts post potassium stimulation compared to RNAi Controls. Statistically significant changes are highlighted in orange color. Wilcoxon rank sum test p-values are reported. N = 30(*alpha-Cat*-RNAi), 30(*Atpalpha*-RNAi), 58(*Flo-2*-RNAi), 28(*Vha55*-RNAi), 98(*gs2*-RNAi), 238(*Lac*-RNAi), 48(*Nrg*-RNAi), 73(*nrv2*-RNAi), 114(*Pdi*-RNAi), 76(*shot*-RNAi) NMJs) **C)** Confocal images showing representative control **(i-iii)** and *gs2*-RNAi **(iv-vi)** synapses from the spaced potassium assay experiment. Axon terminal and ghost boutons are labelled in green, and the anti-Discs-large antibody labelling in magenta

in i) and iv). ii) and iii) represent the area inside the white rectangle in i) (see in-image labels for details). v) and vi) represent the area inside the white rectangle in iv). ii) and iii) show multiple ghost boutons lacking the post-synaptic density for the Control panel indicated with orange asterisks. v) and vi) show an extreme case where no ghost boutons were found for that NMJ is presented for the *gs2*-RNAi panel. **D)** Confocal images showing representative control (i-iii) and *shot*-RNAi (iv-vi) synapses (see in-image labels for details). NMJ glial projections for *shot*-RNAi (iv) are much less expansive than the control in the unstimulated NMJs (i). **E)** Confocal images showing representative control (i) and *Pdi*-RNAi (ii) synapses (see in-image labels for details). The NMJ areas are much smaller for the *Pdi*-RNAi NMJs when compared to the control in the stimulated NMJs. **F-G)** Foldchange in glial protrusion area, neurite area and their ratio upon knock-down of glial protrusion-localized transcripts before (F, N = 28(*alpha-Cat*-RNAi), 30(*Atpalpha*-RNAi), 30(*Flo-2*-RNAi), 23(*Vha55*-RNAi), 30(*gs2*-RNAi), 28(*Lac*-RNAi), 23(*Nrg*-RNAi), 28(*nrv2*-RNAi), 28(*Pdi*-RNAi), 27(*shot*-RNAi) NMJs)) and after (G, N = 30(*alpha-Cat*-RNAi), 30(*Atpalpha*-RNAi), 58(*Flo-2*-RNAi), 28(*Vha55*-RNAi), 97(*gs2*-RNAi), 239(*Lac*-RNAi), 48(*Nrg*-RNAi), 73(*nrv2*-RNAi), 114(*Pdi*-RNAi), 79(*shot*-RNAi) NMJs)) potassium activation assay. Data represents average foldchange for each gene. Student's t-test.

Figure S5. Knockdown of *Vha55* causes a small larval brain phenotype. Confocal images showing the marked difference in size between the A) control (Repo-GAL4>UAS-mCD8-GFP; UAS-*mCherry*-RNAi) and B) *Vha55*-RNAi (Repo-GAL4>UAS-mCD8-GFP;UAS-*Vha55*-RNAi) brains for 3rd instar larvae of very similar sizes (representative of 5 brains for each condition).

Figure 1

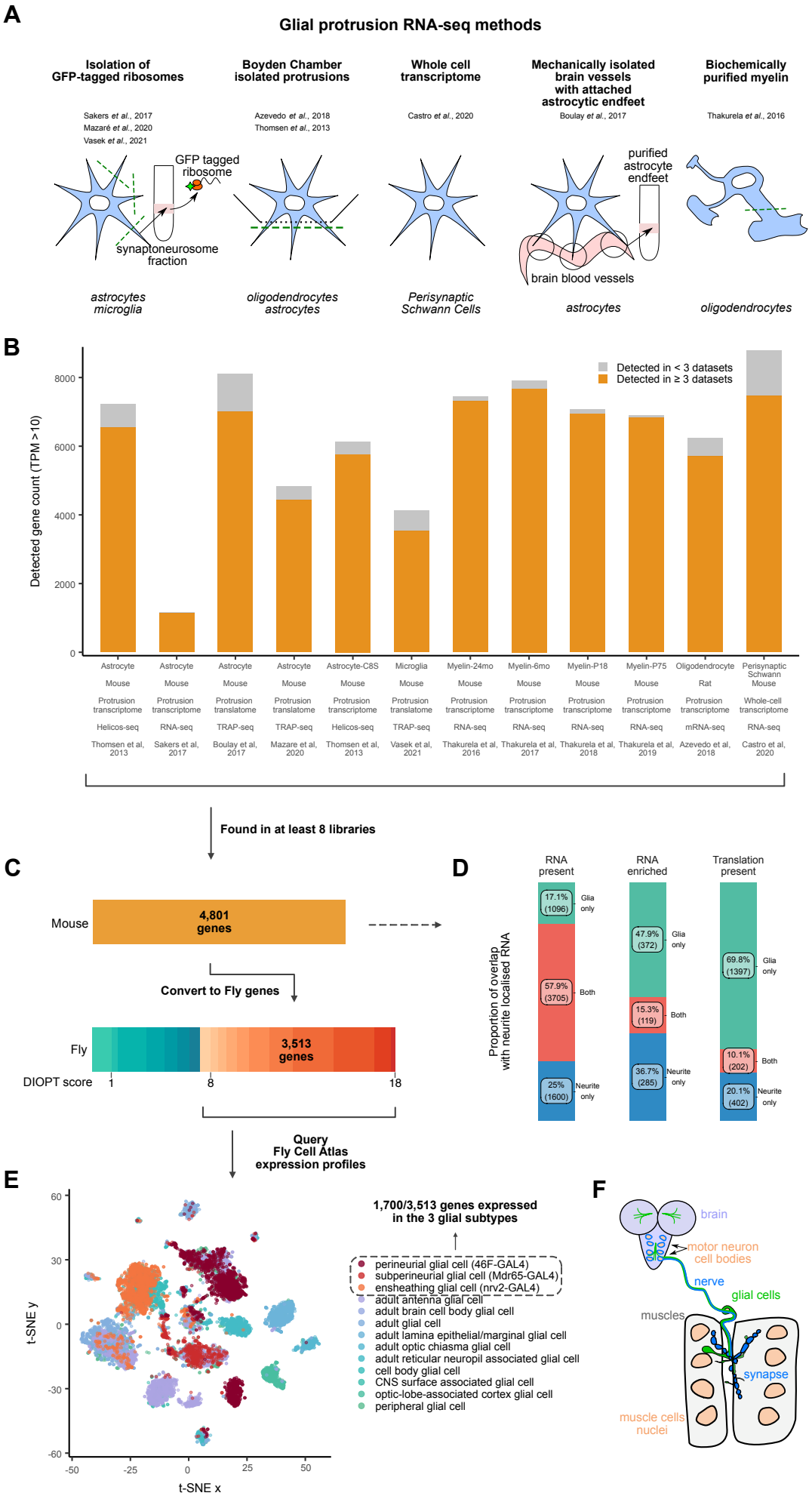
A
Glial protrusion RNA-seq methods
Isolation of GFP-tagged ribosomes
Sakers et al., 2017
Mazaré et al., 2020
Vasek et al., 2021
GFP tagged ribosome
synaptoneurosome fraction
astrocytes microglia
Boyden Chamber isolated protrusions
Azevedo et al., 2018
Thomsen et al., 2013
oligodendrocytes astrocytes
Whole cell transcriptome
Castro et al., 2020
Perisynaptic Schwann Cells
Mechanically isolated brain vessels with attached astrocytic endfeet
Boulay et al., 2017
purified astrocyte endfeet
brain blood vessels
astrocytes
Biochemically purified myelin
Thakurela et al., 2016
oligodendrocytes
B
Detected gene count (TPM >10)
Detected in < 3 datasets
Detected in ≥ 3 datasets
Astrocyte Mouse Protrusion transcriptome Helicos-seq Thomsen et al, 2013
Astrocyte Mouse Protrusion transcriptome RNA-seq Sakers et al, 2017
Astrocyte Mouse Protrusion translatome TRAP-seq Boulay et al, 2017
Astrocyte Mouse Protrusion translatome TRAP-seq Mazare et al, 2020
Astrocyte-C8S Mouse Protrusion transcriptome Helicos-seq Thomsen et al, 2013
Microglia Mouse Protrusion translatome TRAP-seq Vasek et al, 2021
Myelin-24mo Mouse Protrusion transcriptome RNA-seq Thakurela et al, 2016
Myelin-6mo Mouse Protrusion transcriptome RNA-seq Thakurela et al, 2017
Myelin-P18 Mouse Protrusion transcriptome RNA-seq Thakurela et al, 2018
Myelin-P75 Mouse Protrusion transcriptome RNA-seq Thakurela et al, 2019
Oligodendrocyte Rat Protrusion transcriptome mRNA-seq Azevedo et al, 2018
Perisynaptic Schwann Mouse Whole-cell transcriptome RNA-seq Castro et al, 2020
Found in at least 8 libraries
C
Mouse
4,801 genes
Convert to Fly genes
Fly
3,513 genes
DIOPT score
Query Fly Cell Atlas expression profiles
D
RNA present
RNA enriched
Translation present
Proportion of overlap with neurite localised RNA
17.1% (1096) Glia only
57.9% (3705) Both
25% (1600) Neurite only
47.9% (372) Glia only
15.3% (119) Both
36.7% (285) Neurite only
69.8% (1397) Glia only
10.1% (202) Both
20.1% (402) Neurite only
E
t-SNE y
t-SNE x
1,700/3,513 genes expressed in the 3 glial subtypes
perineurial glial cell (46F-GAL4)
subperineurial glial cell (Mdr65-GAL4)
ensheathing glial cell (nrv2-GAL4)
adult antenna glial cell
adult brain cell body glial cell
adult glial cell
adult lamina epithelial/marginal glial cell
adult optic chiasma glial cell
adult reticular neuropil associated glial cell
cell body glial cell
CNS surface associated glial cell
optic-lobe-associated cortex glial cell
peripheral glial cell
F
brain
motor neuron cell bodies
nerve
glial cells
muscles
synapse
muscle cells nuclei

Figure S1

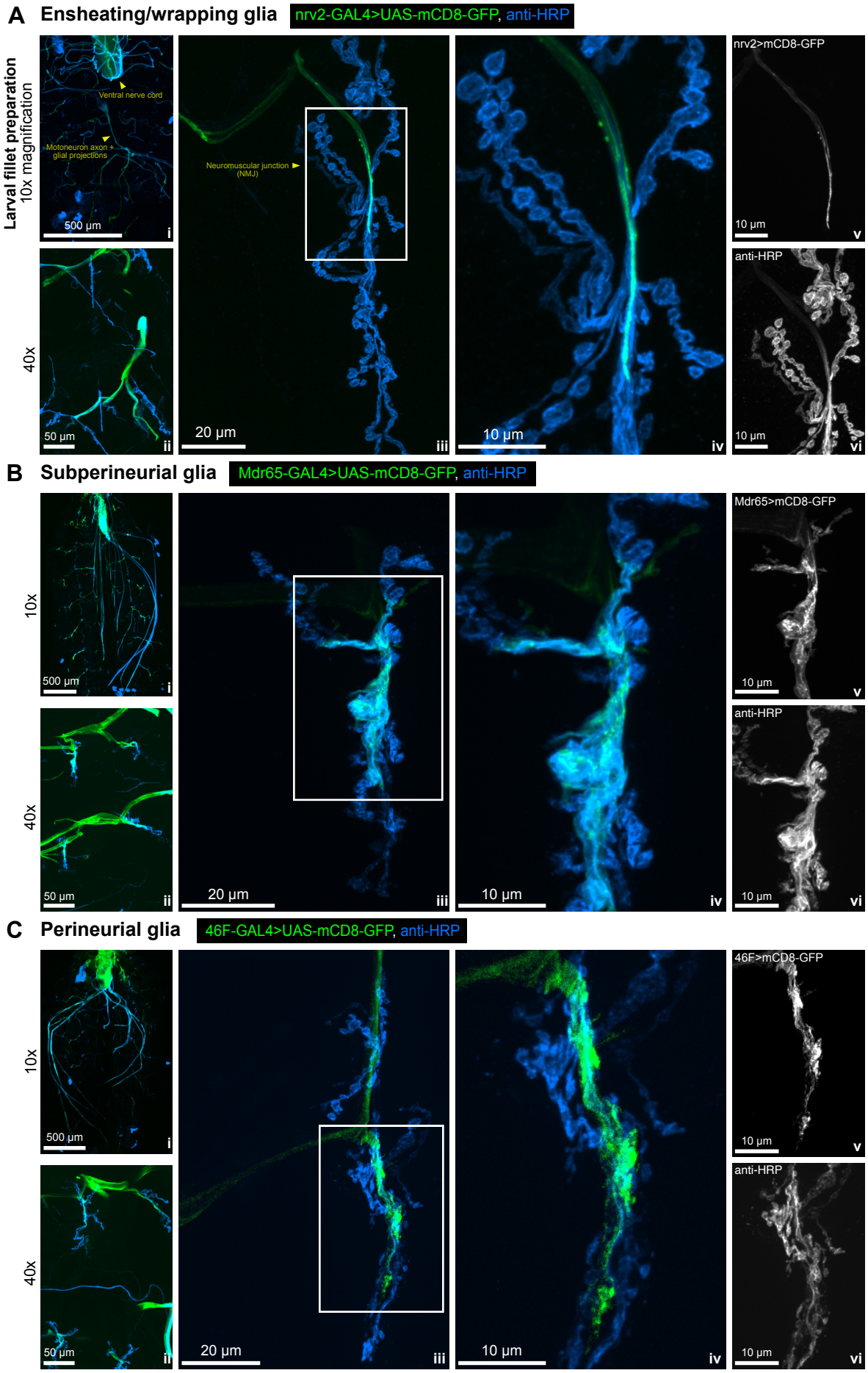
A Ensheating/wrapping glia
nrv2-GAL4>UAS-mCD8-GFP, anti-HRP
Larval fillet preparation
10x magnification
Ventral nerve cord
Motoneuron axon + glial projections
Neuromuscular junction (NMJ)
500 µm
i
40x
50 µm
ii
20 µm
iii
10 µm
iv
nrv2>mCD8-GFP
10 µm
v
anti-HRP
10 µm
vi
B Subperineurial glia
Mdr65-GAL4>UAS-mCD8-GFP, anti-HRP
10x
500 µm
i
40x
50 µm
ii
20 µm
iii
10 µm
iv
Mdr65>mCD8-GFP
10 µm
v
anti-HRP
10 µm
vi
C Perineurial glia
46F-GAL4>UAS-mCD8-GFP, anti-HRP
10x
500 µm
i
40x
50 µm
ii
20 µm
iii
10 µm
iv
46F>mCD8-GFP
10 µm
v
anti-HRP
10 µm
vi

Figure 2

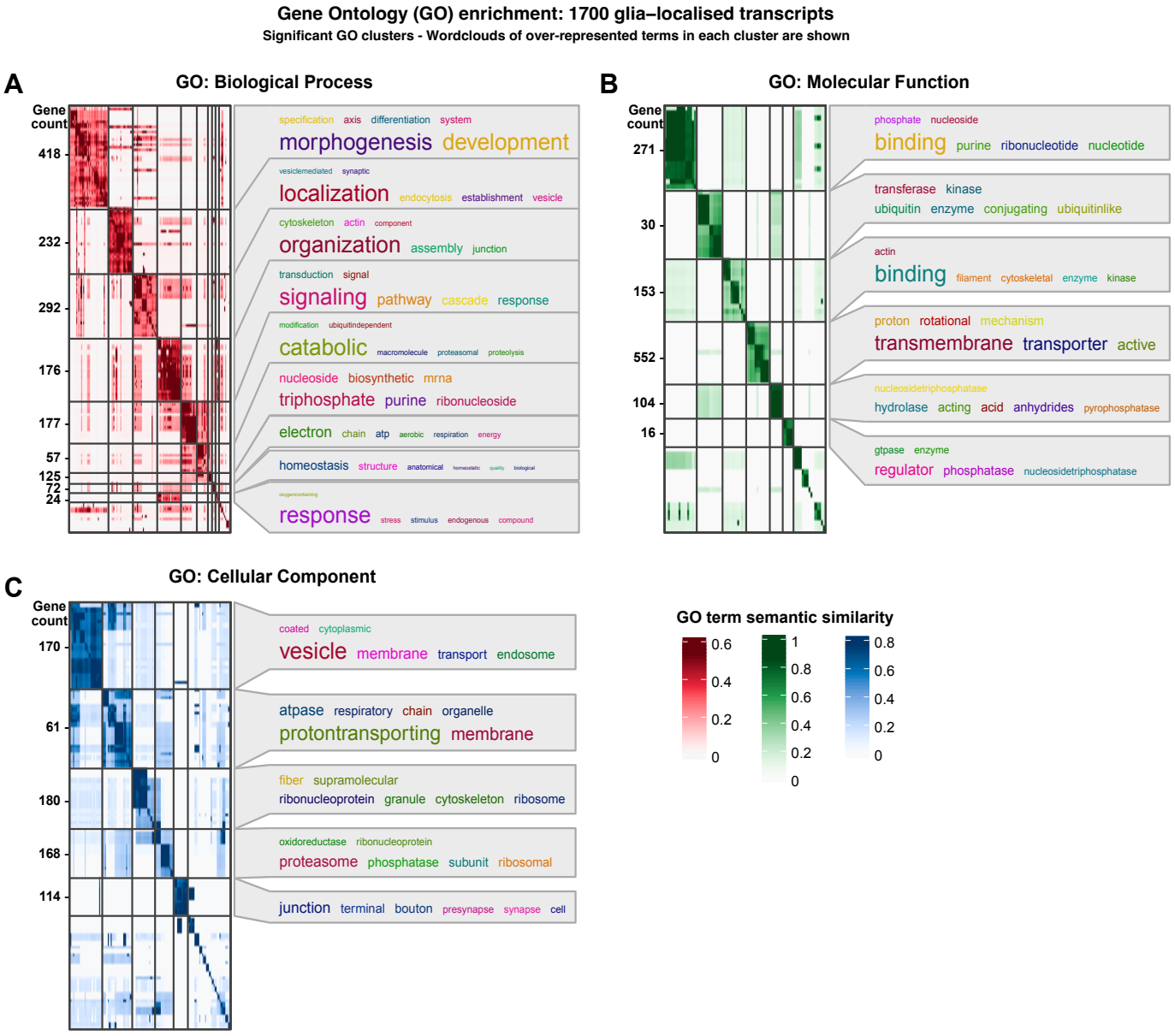
Gene Ontology (GO) enrichment: 1700 glia–localised transcripts
Significant GO clusters - Wordclouds of over-represented terms in each cluster are shown
A
GO: Biological Process
Gene count
418
232
292
176
177
57
125
72
24
specification axis differentiation system
morphogenesis development
vesiclemediated synaptic
localization endocytosis establishment vesicle
cytoskeleton actin component
organization assembly junction
transduction signal
signaling pathway cascade response
modification ubiquitindependent
catabolic macromolecule proteasomal proteolysis
nucleoside biosynthetic mrna
triphosphate purine ribonucleoside
electron chain atp aerobic respiration energy
homeostasis structure anatomical homeostatic quality biological
oxygencontaining
response stress stimulus endogenous compound
B
GO: Molecular Function
Gene count
271
30
153
552
104
16
phosphate nucleoside
binding purine ribonucleotide nucleotide
transferase kinase
ubiquitin enzyme conjugating ubiquitinlike
actin
binding filament cytoskeletal enzyme kinase
proton rotational mechanism
transmembrane transporter active
nucleosidetriphosphatase
hydrolase acting acid anhydrides pyrophosphatase
gtpase enzyme
regulator phosphatase nucleosidetriphosphatase
C
GO: Cellular Component
Gene count
170
61
180
168
114
coated cytoplasmic
vesicle membrane transport endosome
atpase respiratory chain organelle
protontransporting membrane
fiber supramolecular
ribonucleoprotein granule cytoskeleton ribosome
oxidoreductase ribonucleoprotein
proteasome phosphatase subunit ribosomal
junction terminal bouton presynapse synapse cell
GO term semantic similarity
0.6
0.4
0.2
0
1
0.8
0.6
0.4
0.2
0
0.8
0.6
0.4
0.2
0

Figure S2

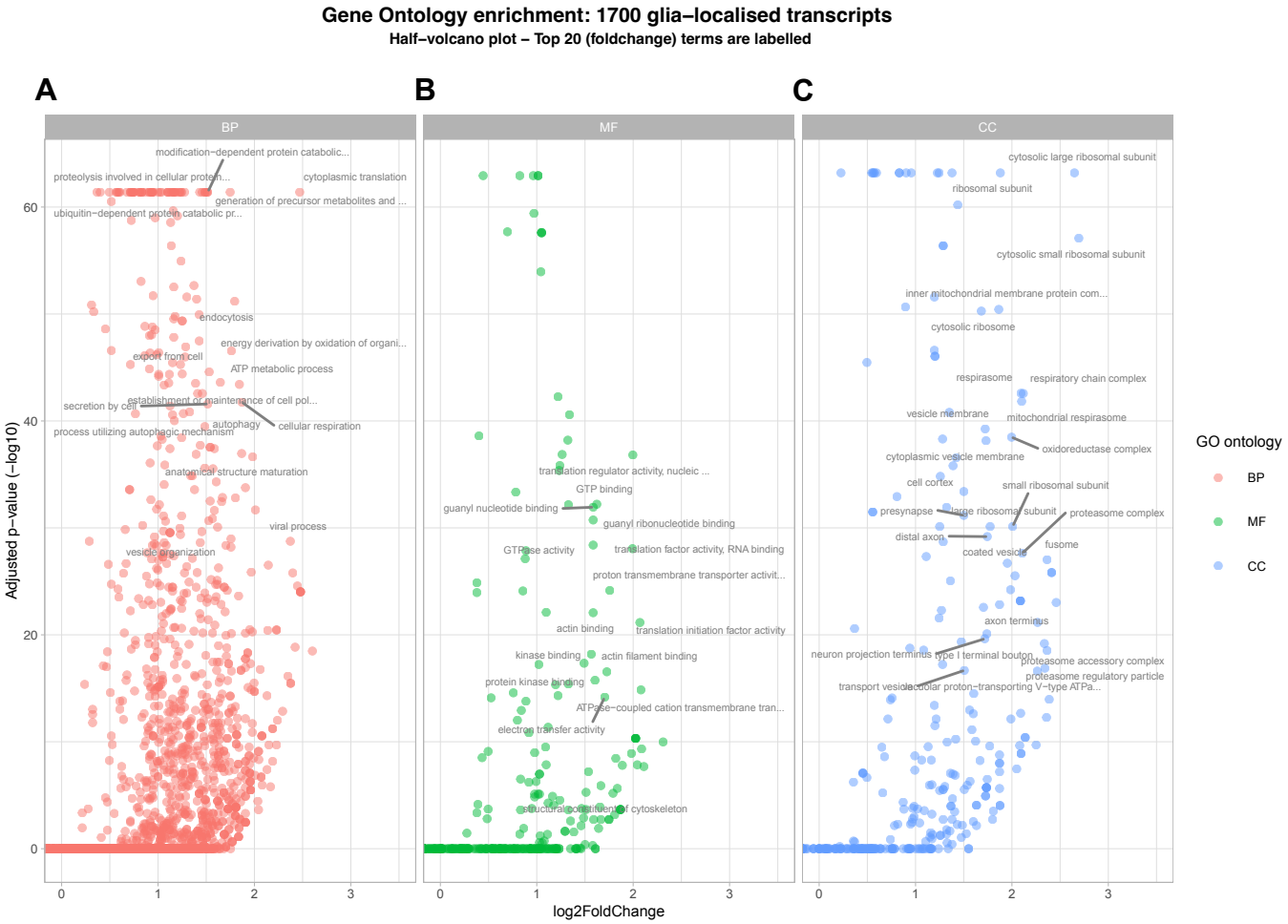
Gene Ontology enrichment: 1700 glia−localised transcripts
Half−volcano plot – Top 20 (foldchange) terms are labelled
A
B
C
BP
MF
CC
modification−dependent protein catabolic...
proteolysis involved in cellular protein...
cytoplasmic translation
generation of precursor metabolites and ...
ubiquitin−dependent protein catabolic pr...
endocytosis
energy derivation by oxidation of organi...
export from cell
ATP metabolic process
establishment or maintenance of cell pol...
secretion by cell
autophagy
cellular respiration
process utilizing autophagic mechanism
anatomical structure maturation
viral process
vesicle organization
translation regulator activity, nucleic ...
GTP binding
guanyl nucleotide binding
guanyl ribonucleotide binding
GTPase activity
translation factor activity, RNA binding
proton transmembrane transporter activit...
actin binding
translation initiation factor activity
kinase binding
actin filament binding
protein kinase binding
ATPase−coupled cation transmembrane tran...
electron transfer activity
structural constituent of cytoskeleton
cytosolic large ribosomal subunit
ribosomal subunit
cytosolic small ribosomal subunit
inner mitochondrial membrane protein com...
cytosolic ribosome
respirasome
respiratory chain complex
vesicle membrane
mitochondrial respirasome
oxidoreductase complex
cytoplasmic vesicle membrane
cell cortex
small ribosomal subunit
presynapse
large ribosomal subunit
proteasome complex
distal axon
coated vesicle
fusome
axon terminus
neuron projection terminus type I terminal bouton
proteasome accessory complex
proteasome regulatory particle
transport vesicle
vacuolar proton−transporting V−type ATPa...
Adjusted p−value (−log10)
log2FoldChange
GO ontology
BP
MF
CC

Figure 3

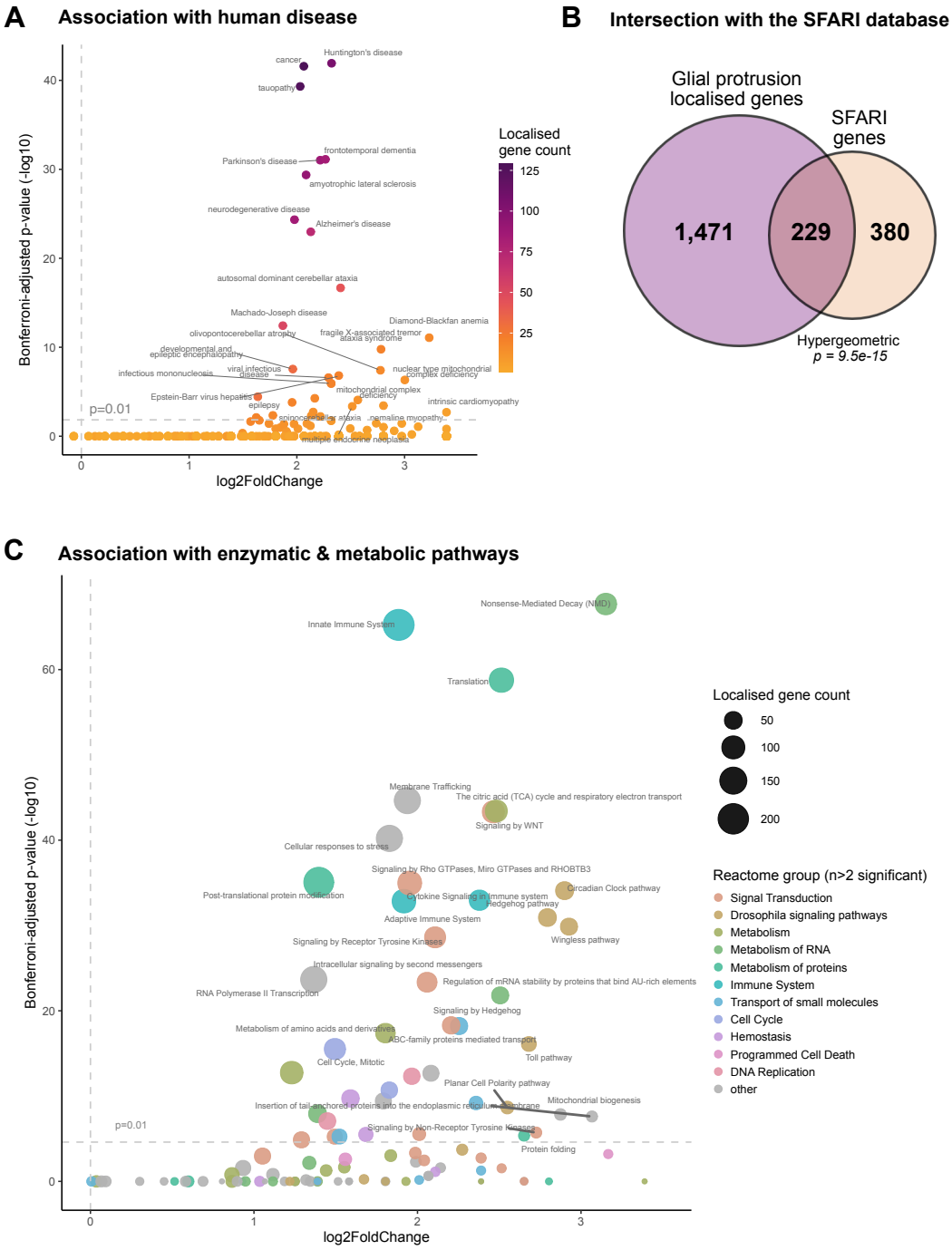
A
Association with human disease
Bonferroni-adjusted p-value (-log10)
log2FoldChange
Localised gene count
125
100
75
50
25
Huntington's disease
cancer
tauopathy
frontotemporal dementia
Parkinson's disease
amyotrophic lateral sclerosis
neurodegenerative disease
Alzheimer's disease
autosomal dominant cerebellar ataxia
Machado-Joseph disease
Diamond-Blackfan anemia
olivopontocerebellar atrophy
fragile X-associated tremor ataxia syndrome
developmental and epileptic encephalopathy
infectious mononucleosis
viral infectious disease
nuclear type mitochondrial complex deficiency
mitochondrial complex deficiency
Epstein-Barr virus hepatitis
epilepsy
intrinsic cardiomyopathy
nemaline myopathy
multiple endocrine neoplasia
p=0.01
B
Intersection with the SFARI database
Glial protrusion localised genes
SFARI genes
1,471
229
380
Hypergeometric
p = 9.5e-15
C
Association with enzymatic & metabolic pathways
Bonferroni-adjusted p-value (-log10)
log2FoldChange
Nonsense-Mediated Decay (NMD)
Innate Immune System
Translation
Membrane Trafficking
The citric acid (TCA) cycle and respiratory electron transport
Signaling by WNT
Cellular responses to stress
Signaling by Rho GTPases, Miro GTPases and RHOBTB3
Post-translational protein modification
Cytokine Signaling in Immune system
Circadian Clock pathway
Hedgehog pathway
Adaptive Immune System
Wingless pathway
Signaling by Receptor Tyrosine Kinases
Intracellular signaling by second messengers
Regulation of mRNA stability by proteins that bind AU-rich elements
RNA Polymerase II Transcription
Signaling by Hedgehog
Metabolism of amino acids and derivatives
ABC-family proteins mediated transport
Toll pathway
Cell Cycle, Mitotic
Planar Cell Polarity pathway
Mitochondrial biogenesis
Insertion of tail-anchored proteins into the endoplasmic reticulum membrane
Signaling by Non-Receptor Tyrosine Kinases
Protein folding
p=0.01
Localised gene count
50
100
150
200
Reactome group (n>2 significant)
Signal Transduction
Drosophila signaling pathways
Metabolism
Metabolism of RNA
Metabolism of proteins
Immune System
Transport of small molecules
Cell Cycle
Hemostasis
Programmed Cell Death
DNA Replication
other

Figure 4

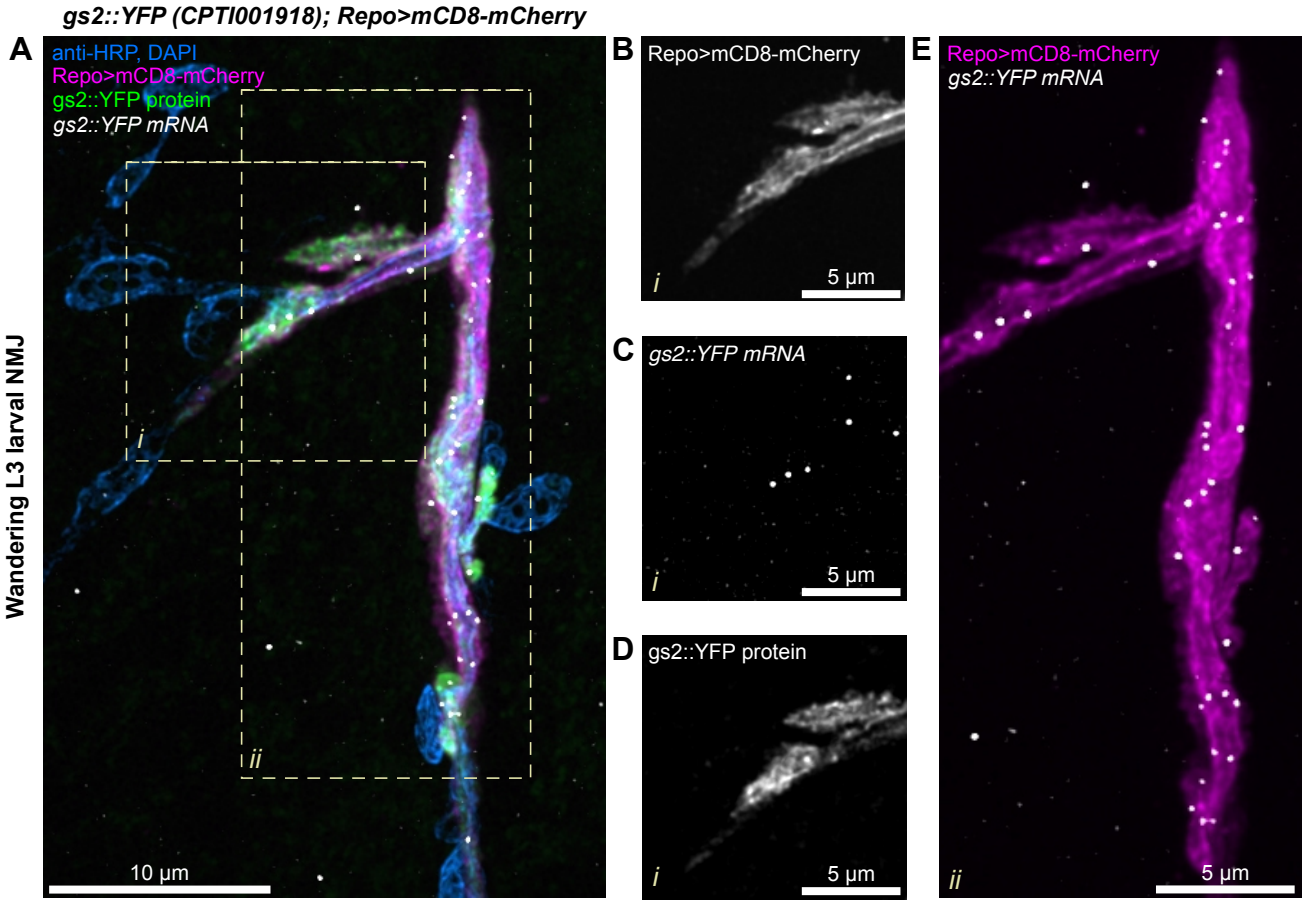
gs2::YFP (CPTI001918); Repo>mCD8-mCherry
Wandering L3 larval NMJ
A
anti-HRP, DAPI
Repo>mCD8-mCherry
gs2::YFP protein
gs2::YFP mRNA
i
ii
10 µm
B
Repo>mCD8-mCherry
i
5 µm
C
gs2::YFP mRNA
i
5 µm
D
gs2::YFP protein
i
5 µm
E
Repo>mCD8-mCherry
gs2::YFP mRNA
ii
5 µm

Figure S4

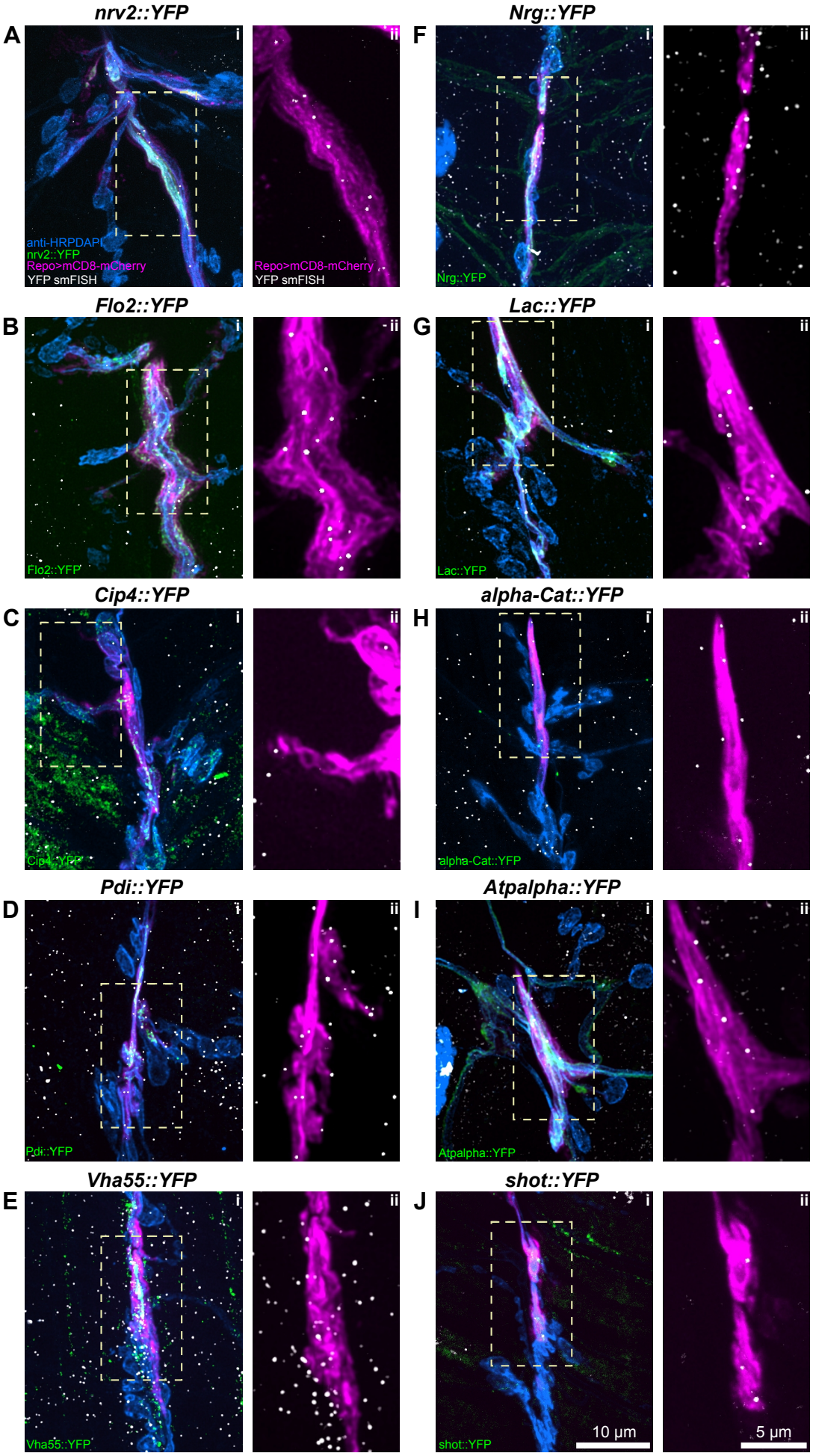
nrv2::YFP
A
i
ii
anti-HRPDAPI
nrv2::YFP
Repo>mCD8-mCherry
YFP smFISH
Repo>mCD8-mCherry
YFP smFISH
Nrg::YFP
F
Nrg::YFP
Flo2::YFP
B
Flo2::YFP
Lac::YFP
G
Lac::YFP
Cip4::YFP
C
Cip4::YFP
alpha-Cat::YFP
H
alpha-Cat::YFP
Pdi::YFP
D
Pdi::YFP
Atpalpha::YFP
I
Atpalpha::YFP
Vha55::YFP
E
Vha55::YFP
shot::YFP
J
shot::YFP
10 µm
5 µm

Figure 5

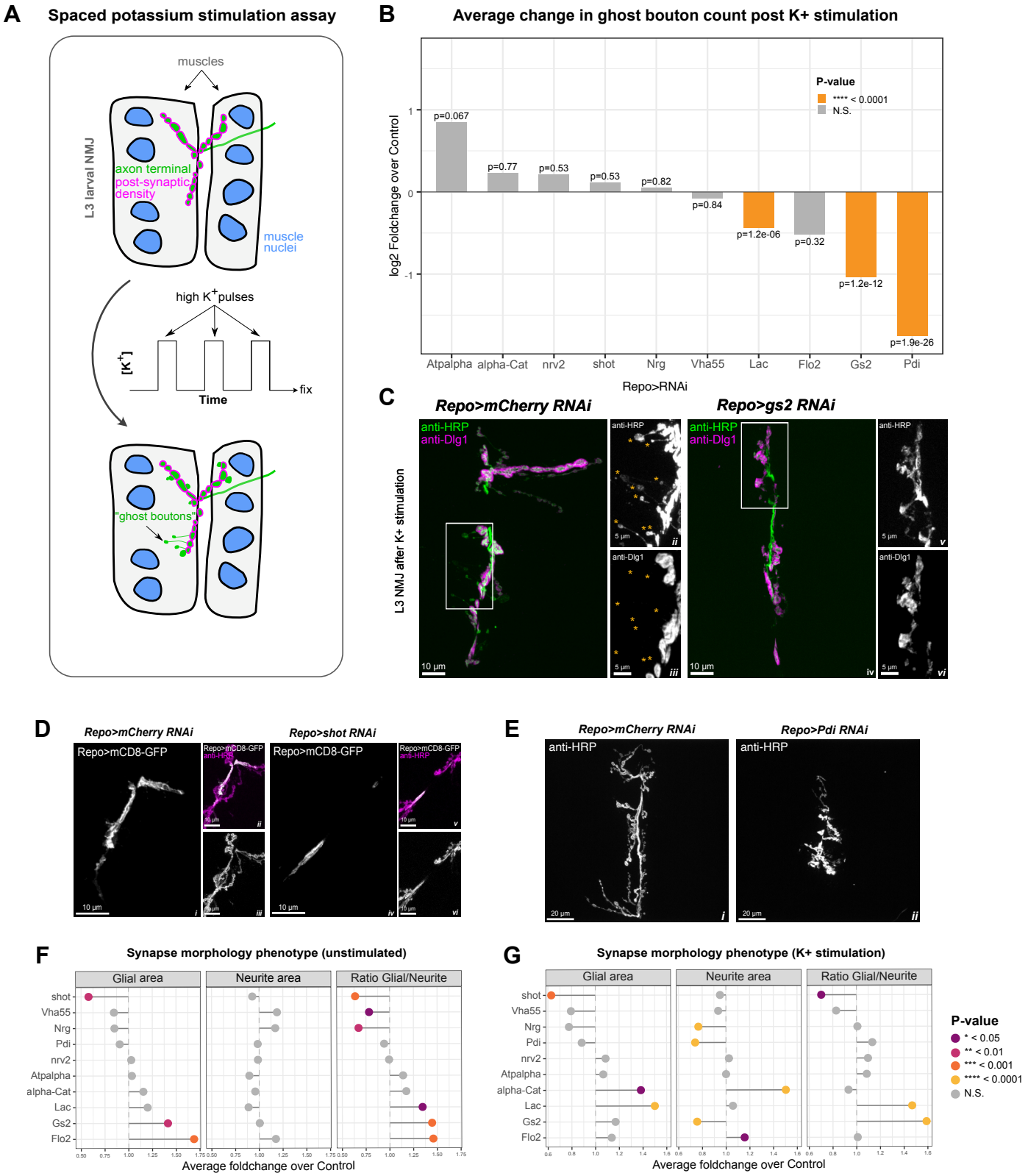
A
Spaced potassium stimulation assay
muscles
L3 larval NMJ
axon terminal
post-synaptic density
muscle nuclei
high K+ pulses
[K+]
Time
fix
"ghost boutons"
B
Average change in ghost bouton count post K+ stimulation
log2 Foldchange over Control
P-value
**** < 0.0001
N.S.
p=0.067
p=0.77
p=0.53
p=0.53
p=0.82
p=0.84
p=1.2e-06
p=0.32
p=1.2e-12
p=1.9e-26
Atpalpha
alpha-Cat
nrv2
shot
Nrg
Vha55
Lac
Flo2
Gs2
Pdi
Repo>RNAi
C
Repo>mCherry RNAi
Repo>gs2 RNAi
L3 NMJ after K+ stimulation
anti-HRP
anti-Dlg1
10 µm
5 µm
D
Repo>mCherry RNAi
Repo>shot RNAi
Repo>mCD8-GFP
E
Repo>mCherry RNAi
Repo>Pdi RNAi
anti-HRP
20 µm
F
Synapse morphology phenotype (unstimulated)
Glial area
Neurite area
Ratio Glial/Neurite
shot
Vha55
Nrg
Pdi
nrv2
Atpalpha
alpha-Cat
Lac
Gs2
Flo2
Average foldchange over Control
G
Synapse morphology phenotype (K+ stimulation)
P-value
* < 0.05
** < 0.01
*** < 0.001
**** < 0.0001
N.S.

Figure S5

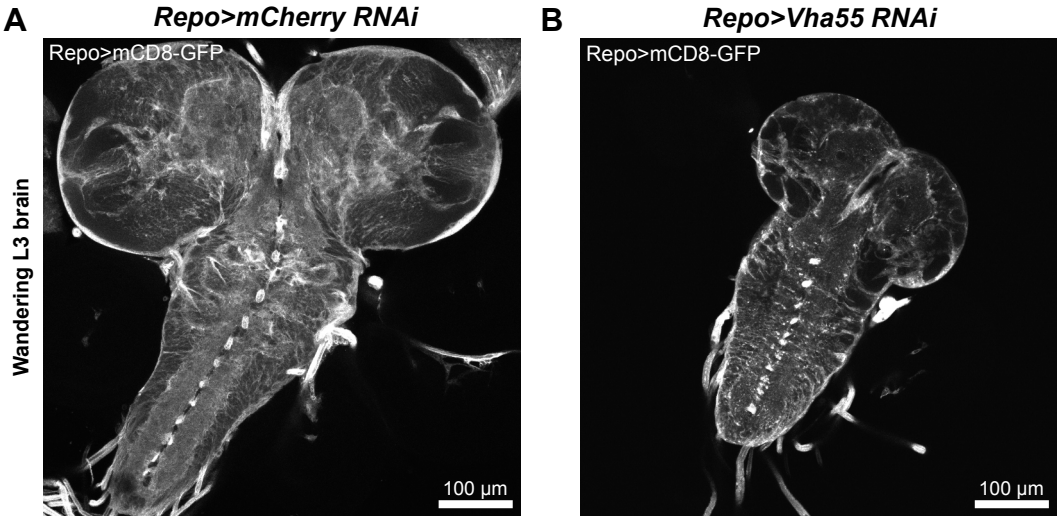
A
Repo>mCherry RNAi
Repo>mCD8-GFP
100 µm
B
Repo>Vha55 RNAi
Repo>mCD8-GFP
100 µm
Wandering L3 brain